UNIVERSITY OF HELSINKI REPORT SERIES IN PHYSICS

HU-P-D97

Molecular dynamics studies of the chemical sputtering of carbon-based materials by hydrogen bombardment

Emppu Salonen

Accelerator Laboratory
Department of Physical Sciences
Faculty of Science
University of Helsinki
Helsinki, Finland

ACADEMIC DISSERTATION

To be presented, with the permission of the Faculty of Science of the University of Helsinki, for public criticism in the Small Auditorium E204 of the Department of Physical Sciences, on August 17th, 2002, at 12 o'clock noon.

HELSINKI 2002

ISBN 951-45-8958-0 (printed version)
ISSN 0356-0961
Helsinki 2002
Yliopistopaino

ISBN 951-45-8959-9 (PDF version)
http://ethesis.helsinki.fi/
Helsinki 2002
Helsingin yliopiston verkkojulkaisut

E. Salonen: **Molecular dynamics studies of the chemical sputtering of carbon-based materials by hydrogen bombardment**, University of Helsinki, 2002, 44 p.+appendices, University of Helsinki Report Series in Physics, HU-P-D97, ISSN 0356-0961, ISBN 951-45-8958-0 (printed version), ISBN 951-45-8959-9 (PDF version)

Classification (INSPEC): A3410, A7920N
Keywords: Molecular dynamics, chemical sputtering, amorphous carbon, tokamak

ABSTRACT

A central issue in the performance of tokamak fusion devices is the choice of the plasma-facing materials. During the device operation the plasma-facing surfaces are subject to extreme heat and particle loads, as they are impinged on by escaped fusion plasma particles. Although carbon-based materials have excellent thermomechanical properties in view of the high heat flux, their use in the next-step fusion device ITER is restricted by high chemical sputtering yields by the impinging hydrogen even at energies as low as a few eV's. The exact mechanism of the chemical sputtering has not been known.

Using molecular dynamics simulations we have studied the erosion of amorphous hydrogenated carbon surfaces by low-energy ($\leq$ 35 eV) hydrogenic atoms. The main finding of this thesis is a new sputtering mechanism, where an impinging hydrogen atom breaks the covalent bond between two carbon atoms by penetrating the region between them. This mechanism was first observed in simulations employing an empirical force model and was later verified with more accurate tight-binding calculations.

The temperature and energy dependencies of the chemical sputtering were studied. A good overall agreement with experimental data was obtained. Our simulations also provided predictions of the carbon sputtering yields for lower hydrogen impact energies than those achieved in experiments. The experimentally observed isotope effect of the chemical sputtering was explained.

Finally, the effect of Si doping on the chemical sputtering of carbon was studied. It was observed that the C sputtering yield decreases nonlinearly with increasing Si concentration. The inclusion of silicon was concluded to suppress the bond breaking in the C-Si network and enhance the rebonding of unbound hydrocarbon species.

CONTENTS

1 INTRODUCTION

The World Energy Council (WEC) estimates that by the year 2050 the world energy consumption has increased by 60 – 160% from the level of 1990 [1]. The reasons for this are clear: growing world population and the industrialization of developing countries. Although the geological resources for fossil fuels are still abundant, only a part of them can be exploited with the current technology. Furthermore, the use of fossil fuels is subject to increasing criticism due to the release of carbon dioxide on their burning. It is presumed that technology for the use of renewable energy sources (*i.e.* hydroelectric, solar, wind, geothermal, biomass) will develop to meet a larger portion of the global energy consumption. However, there is no indication that the renewable energy sources would be able to satisfy the total demand.

One of the alternative sources of energy is the thermonuclear fusion of light nuclei. Similar reactions take place in the sun, releasing tremendous amounts of energy [2]. In comparison with the fossil fuel and nuclear (fission-based) power production, fusion technology is environmentally safe and no long-term storage for the produced radioactive waste is required [3].

The most successful fusion reactor experiments are the tokamaks, in which the fusion plasma is controlled by magnetic fields and confined in a toroidal vessel. After 50 years of research and development on harnessing thermonuclear fusion for energy production, the tokamak fusion technology is finally entering a demonstrative phase. With the construction of ITER (International Thermonuclear Experimental Reactor; also Latin for 'the way'), the first next-generation tokamak, a clear proof of the feasibility of fusion-based power production is expected [3, 4].

One of the critical problems for the development of commercially viable fusion technology is the choice of the plasma-facing components (PFCs). Although the fusion plasma is confined at the center of the vacuum chamber, some of the plasma particles leak outside the closed magnetic field lines and interact with the chamber walls. In tokamaks, specifically chosen wall structures are used to handle the boundary plasma. The term 'first wall' is used to distinguish the plasma-facing armour material from the actual walls of the vacuum chamber.

The most severe damage to the first wall is caused by the intense ($\sim 10^{22}$ – 10^{24} ions/m^{2}s) bombardment by hydrogenic particles. This leads to the erosion of the PFCs, degradation of their thermal and mechanical properties, and deposition of the radioactive tritium in the wall structures [5–8]. The fusion plasma purity, on the other hand, will be compromised as eroded impurity species from the PFCs enter the plasma and dilute it. Radiation losses, proportional to the atomic number Z of the impurity species ($\propto Z^2$ to Z^4 [9, 10]) further lead to cooling of the plasma and the extinction of the fusion reaction.

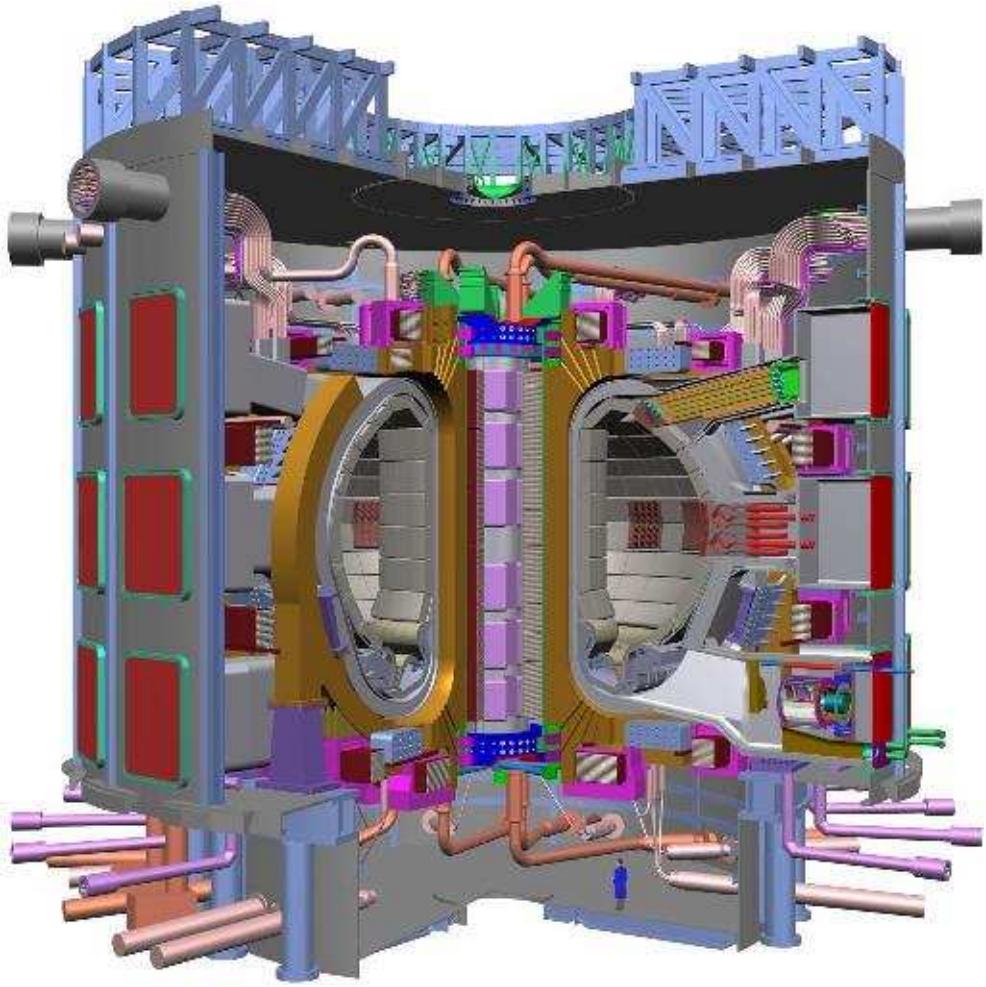

Figure 1: Schematic view of the ITER tokamak. The D-shaped cross section of the vacuum chamber can be seen at the center. Picture published with the kind permission of ITER [3].

During the last decades, carbon has been one of the most promising first wall materials. Although carbon has excellent thermal and mechanical properties, chemical erosion by oxygen and more importantly hydrogen atoms and ions, results in too high erosion rates for long-term operation [11]. Moreover, hydrocarbon species released from the first wall surfaces form C:T films upon redeposition. This leads to the accumulation of a harmful tritium inventory in the vessel walls.

According to the current ITER design carbon will only be used in the high heat flux components [4], while tungsten and beryllium will be used elsewhere in the first wall. However, both beryllium and tungsten have their disadvantages. Beryllium has a very high erosion rate [12] under tokamak-relevant conditions and melts easily. While the erosion of tungsten under the hydrogen bombardment is negligible, several other mechanisms contribute to W erosion in fusion devices: arcing [13], blistering [14], and sputtering by redeposited W species [15, 16], which could be enhanced due to lowering of the threshold energy of sputtering by oxygen [17]. Furthermore, W ions are several orders of magnitude

more harmful plasma impurities than C or Be ions.

There is intense ongoing research for the development of carbon-based plasma-facing materials. The introduction of dopants aims to reduce the tritium retention and chemical sputtering by hydrogen and oxygen, while still retaining the required thermomechanical properties. This research requires the knowledge of the fundamental erosion processes of carbon-based materials, the form in which the hydrocarbon species are released from plasma-facing surfaces, and how laboratory data can be extrapolated to fusion-device-relevant irradiation conditions.

2 PURPOSE AND STRUCTURE OF THIS STUDY

The purpose of this study is to obtain a detailed description of the mechanisms that lead to the chemical sputtering of carbon-based materials under low-energy ($\sim$ 1 – 35 eV) hydrogen irradiation and the factors contributing to them. This knowledge can then aid the development of better plasma-facing materials with the proper choice of dopants and their concentrations, and finding the optimal parameters for the plasmas above the divertor.

This thesis consists of this summary and five articles, which have been published or accepted for publication in refereed international scientific journals. The articles are summarized below and included after the summary. The author has carried out all the empirical potential calculations, most of the data analysis, and written most of the text in papers **I, III – V**. In paper **II** the author contributed to the empirical potential calculations and writing of the text. The tight-binding simulations in paper **II** were carried out by a co-author.

The structure of this summary is as follows. In the current section a brief summary on each article is given. In section 3 the basics on tokamak fusion devices and plasma-divertor interactions are presented. In section 4 an overview of the mechanisms of carbon erosion by hydrogen is given. In section 5 the molecular dynamics method is described, along with the force models used in this study. The results of the molecular dynamics modeling are presented in section 6. Finally, the conclusions and outlook are given in section 7.

Summaries of the original papers

Paper I: Bond-breaking mechanism of sputtering, E. Salonen, K. Nordlund, J. Keinonen, and C. H. Wu, *Europhys. Lett.* **52** (2000) 504.

Chemical sputtering of amorphous hydrogenated carbon by low-energy (5 – 35 eV) hydrogen irradiation is studied. We describe in detail a sputtering mechanism where the impinging hydrogen ion attacks the region between two carbon atoms, breaking the covalent bond and pushing the two carbon atoms apart. Studies on the temperature dependence of the sputtering yield result in a peak around 900 K.

Paper II: Sputtering of amorphous hydrogenated carbon by hyperthermal ions as studied by tight-binding molecular dynamics, A. V. Krasheninnikov, K. Nordlund, E. Salonen, J. Keinonen, and C. H. Wu, *Comput. Mater. Sci.*, accepted for publication.

Tight-binding and empirical force models are employed to determine to which extent quantum-mechanical effects are important for the swift chemical bond breaking. The basic features of the mechanism are illustrated with the fragmentation of a carbon dimer. Sputtering yields are calculated for hydrogenated carbon structures with both force models. Although perfect quantitative agreement is not obtained, the tight-binding model does verify the swift chemical sputtering mechanism. The effect of the C–C interaction range of the empirical model is shown to have an effect on the sputtering yields.

Paper III: Suppression of carbon erosion by hydrogen shielding during high-flux hydrogen bombardment, E. Salonen, K. Nordlund, J. Tarus, T. Ahlgren, J. Keinonen, and C. H. Wu, *Phys. Rev. B* **60** (1999) R14005.

The experimentally observed decrease of the carbon sputtering yield at extremely high flux densities is studied. We show that under low-energy (E_{rms} = 1 eV) hydrogen irradiation, a supersaturated hydrogen concentration in the amorphous carbon network is obtained. The high number of hydrogen atoms at the surface shields the carbon network beneath from the impinging hydrogen, reducing the sputtering yield.

Paper IV: Swift chemical sputtering of amorphous hydrogenated carbon, E. Salonen, K. Nordlund, J. Keinonen, and C. H. Wu, *Phys. Rev. B* **63** (2001) 195415.

The sputtering of amorphous hydrogenated carbon by H, D and T isotopes of hydrogen is studied in the energy range 1 – 35 eV. A clear isotopic effect on the sputtering yield is observed, in agreement with experiments. The supersaturation of the surface hydrogen concentration, first observed in paper **III**, is studied at higher energies. The distributions of the eroded species are determined. Finally, the temperature dependence of the sputtering yield observed in paper **I** is studied in more detail. Both fixed and temperature-dependent values of the hydrogen saturation concentration are used. The sputtering yield maxima are observed between 700 and 900 K.

Paper V: Reduced chemical sputtering of carbon by silicon doping, E. Salonen, K. Nordlund, J.

Keinonen, N. Runeberg, and C. H. Wu, *J. Appl. Phys.*, accepted for publication.

The effect of Si doping on the chemical sputtering of carbon by deuterium is studied. It is observed that the carbon sputtering yield decreases with increasing Si-concentration. The reasons for the reduced sputtering yields are determined to be the long Si–C bonds and dynamic rebonding of unbound hydrocarbon species to Si sites. Comparison between the simulated data and experiment, along with a fit to extrapolate the results to higher Si concentrations, shows a good agreement.

3 MAGNETIC CONFINEMENT FUSION

In this section the basics of the magnetic confinement fusion are first outlined and the tokamak fusion device is presented. We then turn our attention to the plasma-wall interactions and the divertor first wall configuration employed in tokamaks. The suitability of carbon as a divertor material is discussed and results of carbon divertor experiments are presented.

3.1 D–T fusion

The present-day magnetic confinement fusion technology aims to power production utilizing the fusion reaction between the nuclei of two heavy isotopes of hydrogen, namely deuterium (D) and tritium (T), to produce an energetic neutron and a helium nucleus (α) [9],

$$\mathrm{D} + \mathrm{T} \rightarrow \ \alpha\,(3.5\mathrm{MeV}) + \mathrm{n}\,(14.1\mathrm{MeV}).$$

Of all the H/He fusion reactions, this one has the largest cross-section at temperatures attainable in laboratory conditions ($\sim 10^8$ K). However, the ultimate aim of the fusion research is to provide the technology for harnessing other fusion reactions that do not involve the radioactive tritium.

To achieve a self-sustaining fusion plasma, the radiation losses (thermal, braking, recombination and line radiation) must be compensated by the heat produced in collisions between the energetic α-particles and the hydrogenic ions [9, 10]. This can be accomplished only if the ion temperature is high enough and if the plasma density and ion temperature simultaneously exceed limiting values for a characteristic time (the energy confinement time). The α-particles that have cooled down in collisions with the hydrogenic ions radiate energy from the plasma and dilute it. This low-energy fraction of helium in the plasma is called 'helium ash' and its removal is one of the technological obstacles in the development of fusion reactor technology.

The ability of the plasma for a self-sustaining fusion reaction is given by the fusion triple product, which is the product of the plasma density, ion temperature and energy confinement time. Present-day fusion devices cannot produce a self-sustaining fusion plasma and have to be heated externally. This heating is either accomplished by the injection of a beam of energetic hydrogen atoms, radio/microwave resonance heating, driving a current through the plasma (inductive heating) or magnetic compression of the plasma. When the fusion plasma produces as much power as externally is put into its heating, the break-even condition is met. The term 'ignition' is used when a self-sustaining plasma is achieved only with the energy produced in collisions between the α-particles and the hydrogenic ions.

3.1.1 Fusion power production

The actual power production in future fusion reactors will be due to the energetic neutrons [3]. As they are not bound by the magnetic fields, they escape the core plasma and penetrate the wall structures, where their energy is stored in a special material component called the blanket. The heat produced by the slowing down of the neutrons in the blanket will be used to drive steam turbines in the same fashion as is done in conventional power plants today.

The plentitude of the fusion fuel is one of its attractive factors: roughly 0.015% of the hydrogen in ordinary sea water is deuterium, which practically means a fuel supply for millions of years. The other fuel component, tritium, is not found in nature but can be produced in laboratory conditions from nuclear reactions between lithium nuclei and a beam of energetic neutrons. Also, future fusion power plants will be able to use the neutrons from the fusion reaction itself to interact with blanket structures made of lithium ('breeders') to produce tritium.

The fusion technology is much cleaner than the technology utilizing fossil fuels, as there is no pollution of the atmosphere caused by combustion products. It is also much safer than fission technology, since a possible operation failure only results in a rapid shutdown of the fusion reaction. However, tritium is a radioactive gas and contaminates the vessel walls during the device operation [18]. Tritium can easily spread both air- and waterborne, posing a safety hazard for the operation personnel. Also, low activation blanket materials need to be used to avoid the radioactivity induced by the fast neutrons. The storage time for the activated materials is short ($\sim$50 – 100 years) compared with the time scales relevant for the fission reactor waste (of the order of $\sim$10 000 years).

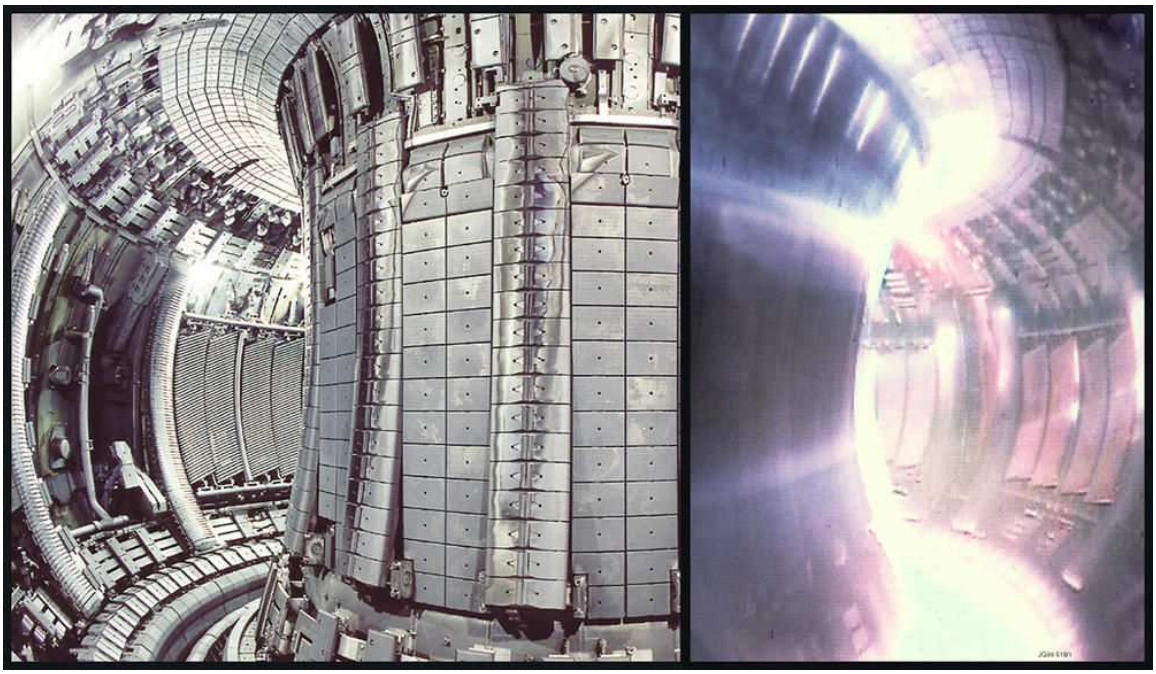

Figure 2: View from inside the torus of JET (Joint European Torus), the largest existing tokamak. The image is split showing the wall structures on the left and the plasma during the device operation on the right. Photographs courtesy of EFDA-JET.

3.2 Tokamak

Originally of Soviet design, the tokamaks [19] are the most widely used and technologically most developed fusion research devices. During the last 35 years of research the fusion triple product achieved in tokamaks has improved by more than four orders of magnitude, reaching the ignition conditions within a factor of 6. The first next-generation tokamak, ITER, will be the first machine large enough for a self-sustaining fusion plasma, and aims for a fusion power gain (*i.e.* the ratio of power produced by the fusion plasma to the external heating power) of 5 – 10, depending on the operation scenario [4]. However, it should be mentioned that pure deuterium plasma experiments with JET have already reached plasma states that would lead to break-even with a D–T fuel.

In tokamak devices the fusion plasma is confined in a toroidal vacuum chamber by the superposition of three magnetic fields: one produced by a set of toroidal coils, one produced by the plasma current itself, and one produced by an auxiliary set of coils to stabilize the position of the plasma in the vessel. Although the tokamaks exhibit excellent confinement properties, some of the plasma particles escape the magnetic confinement and interact with the vessel walls.

The escaped plasma induces an extremely high heat and particle load to material surfaces in contact with it. Not only charged species that follow the magnetic lines, but also neutrals, resulting from

charge exchange reactions, escape the core plasma [10]. Special components, namely limiters and divertors, are used to control the particle flux.

The limiter is essentially a material placed in direct contact with the hot plasma to shape the outer magnetic surface. The limiter is constantly impinged on by energetic plasma particles, resulting in erosion and heating of the material. However, this first wall component has become less important as better plasma energy confinement has been achieved with the divertor.

3.3 Divertor

The divertor is a fusion device component, in which the boundary plasma is directed at two sets of specially selected material plates by magnetic field lines [10]. Before reaching the target plates the density of the plasma increases and it cools down, reducing the power load. Further cooling of the plasma can be achieved by puffing a small amount of gas (*e.g.* Ne, Ar) in the plasma above the divertor plates [4, 20].

As the plasma electrons have higher velocities than the ions, they reach the divertor target plates faster. This results in a negative surface charge on the plates, creating an electric field called the sheath [10]. Before impinging on the divertor plates, the plasma ions are accelerated by the sheath, their energies roughly corresponding to a shifted Maxwellian distribution. The energy shift is proportional to the divertor electron temperature T_e (generally given in eV's), and for hydrogenic ions it is approximately (3–5)$\times T_e$ [21].

Upon reaching the target plates, the ions are neutralized by the excess electrons at the surface. For hydrogenic species, several fundamental interactions are possible: (1) implantation, leading to diffusion and trapping; (2) chemical reactions, such as etching and H_2 formation; and (3) collisions with the surface atoms, leading to ion reflection and/or damage production in the lattice. The mechanisms leading to erosion in the case of (2) and (3) will be described in section 4.

The neutralized plasma species and impurities released from the target plates are finally pumped off from the vacuum chamber. The pumping is essential, as the impurity species can enter the core plasma with deleterious effects. Collisions with the plasma electrons can also ionize the impurity species, which can then be redeposited by the sheath.

Along with enhanced plasma energy confinement, the divertor has other advantages in comparison with the limiter. The charged particles are neutralized away from the core plasma and have a smaller probability of diluting it. Also, the divertor electron temperatures are typically of the order of 1 – 10 eV's, whence the impinging ions have much lower energies. However, due to the intense particle flux,

Figure 3: Divertor target plates in the ASDEX (Axially Symmetric Divertor EXperiment) Upgrade tokamak [22], Garching, Germany.

the nominal thermal load for the divertor target plates in ITER will be roughly 5 MW/m^2, with peaks up to 20 MW/m^2 expected to occur [7, 11]. Hence, only materials with excellent thermal properties and radiation resistance can be used in the divertor.

3.4 Carbon as a divertor material

Carbon-based materials are in many ways ideal PFC materials. They have high thermal conductivities, excellent thermal shock resistance, and do not melt (the sublimation point of graphite is $\sim$ 3640 K [23]). Carbon is a low activation material and its low atomic number makes it possible to tolerate much higher C impurity concentrations in the core plasma, than in the case of high-Z materials like Mo and W. Typically different types of graphite or carbon fiber composites (CFCs) are used in present-day tokamaks.

However, the use of carbon has its problems. Oxygen, the main intrinsic impurity in the vacuum chamber, etches carbon very efficiently with the formation of volatile molecules, such as CO and CO_2. Continuing high-flux bombardment by hydrogen ions and neutrals eventually results in a distorted amorphous hydrogenated carbon (*a*-C:H) structure at the surface of the divertor plates [10], and

estimates of the erosion rates indicate too short operational times for carbon PFCs in actual reactors [4, 11]. Also, hydrocarbon species released from carbon PFCs due to hydrogen bombardment are known to redeposit not only on the divertor plates but in other parts of the vacuum chamber as well [18, 24], forming C:H films. This, in turn, leads to the accumulation of tritium in the vessel walls, when a D–T plasma is used.

3.4.1 Measurements of carbon erosion in tokamaks

Generally, there are three different methods for measuring the carbon erosion yields in tokamaks: optical spectroscopy of photon emissions from dissociated radical species, mass spectroscopy of the partial pressures of different hydrocarbon gases on the vessel walls, and mass loss analysis of the eroded surfaces [21, 25]. The two former methods have the advantage of measuring only chemically eroded species, and optical spectroscopy is widely used for *in situ* measurements of the carbon erosion flux as a function of different plasma parameters.

The different methods quite often lead to qualitatively similar results. Quantitative agreement is not always obtained. The interpretation of the results highly depends on the knowledge of the fundamental erosion processes and distributions of the eroded species [25]. For example, mass loss does not take into account redeposition or make distinction between different erosion mechanisms. On the other hand, mass spectroscopy is usually carried out in the residual gas after the plasma discharge. Thus, radical hydrocarbon species that stick to the vessel walls are not seen with the method.

In optical spectroscopy photon emissions originating from dissociations of hydrocarbon radical species by the plasma particles are measured. The most common measurements are for the photon emissions at 431 nm due to the CH/CD radical dissociations [21, 26–28]. The photon flux is related to the eroded molecular flux with the photon efficiency D/XB, where D and X are the dissociation and excitation rates of the radicals, respectively, and B is the branching ratio into the observed transition. Hence, the quantity D/XB can be thought as the 'molecules per photon' ratio.

Unfortunately, the exact values of D/XB at 431 nm are not well known. Conservatively, for an effective D/XB which takes into account prompt redeposition at the divertor plates, a constant value is assumed [26, 28]. Values depending on the plasma density and T_e have also been suggested [29, 30]. The CH_x/CD_x hydrocarbon species are generally assumed to be the dominant erosion products and their reaction pathways resulting in CH/CD radicals are known. However, the contribution of heavier hydrocarbons (C_yH_x; $y \geq 2$) to the value of D/XB is not known. While it is considered relatively small [29], using the value for only CH_x/CD_x species could result in systematically too low erosion yield estimates.

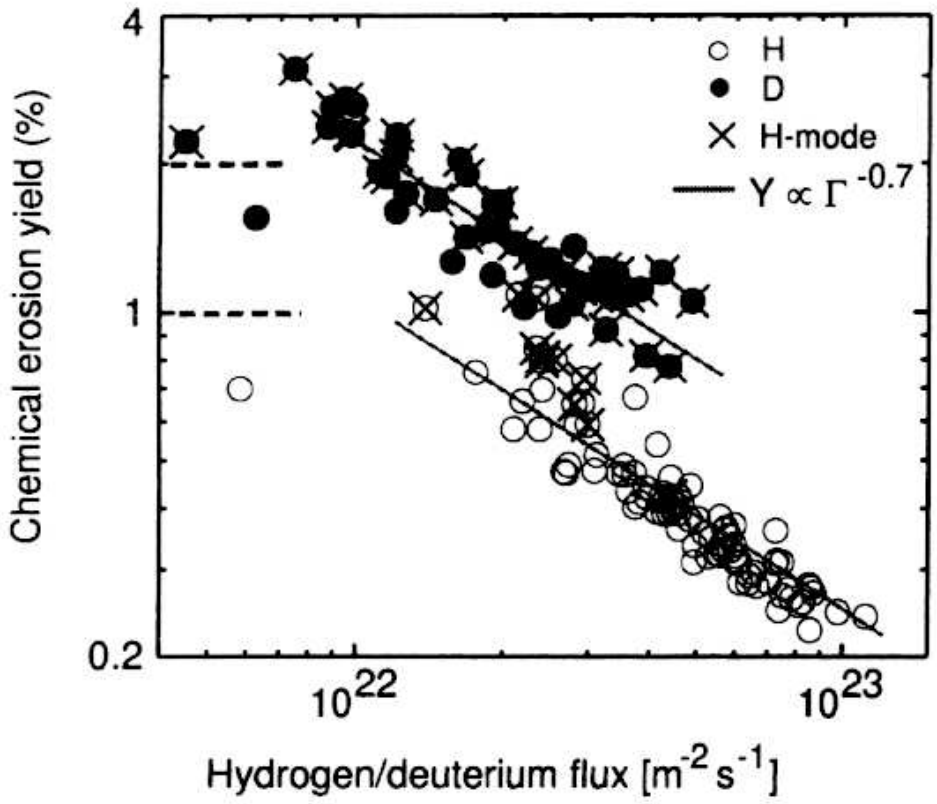

Figure 4: Spectroscopically measured carbon erosion yield as a function of the H/D flux density for different experimental conditions in ASDEX Upgrade. From Ref. [29].

3.4.2 Flux dependence of the chemical erosion of carbon

Reduced carbon erosion yields at extremely high flux densities ($\sim 10^{22}$ – 10^{23} m^{-2}s^{-1}) were recently reported both in tokamaks [26, 28, 29, 31] as well as in plasma simulators [27]. The assumption of a power law dependence $Y \propto \Gamma^{-\alpha}$, where Y is the carbon erosion yield and Γ is the ion flux density, has resulted in values $\alpha \sim 0.4$ – 1.25. This effect could be favorable to the use of carbon divertor plates in ITER where the ion fluxes are estimated to be as high as 10^{24} m^{-2}s^{-1} [7].

There are several problems with the flux dependence measurements. First, the plasma density increases with the ion flux. This results in lower net erosion yields as eroded species are promptly ionized near the divertor surfaces and redeposited. Second, the electron temperature decreases at high flux densities, which could lead to lower erosion yields with decreasing ion impact energies. Experiments with extremely low T_e ($\sim$ 0.25 – 1.2 eV) plasmas resulted in the extinction of the CD band emission [14]. Finally, the values of D/XB at low T_e are now well known and could lead to misinterpretation of the data. An attempt to analyze erosion rate data with values of D/XB varying with plasma density and T_e resulted in unrealistic erosion yields and up to a quadratic flux dependence [32].

4 CARBON EROSION BY HYDROGEN

The interpretation of the experimental data on carbon-based divertor plate erosion in tokamaks requires the knowledge of the fundamental carbon erosion mechanisms. The most important are the mechanisms of erosion by hydrogenic species - not only ionized but also neutral atoms [10]. The best understood of these is physical sputtering, which results in significant erosion at hydrogen impact energies above ∼50 eV [33]. Physical sputtering of carbon occurs also due to bombardment by the helium ash ions but the sputtering yields at divertor-relevant energies are at least an order of magnitude lower than those due to the hydrogenic species [33, 34].

At lower hyperthermal energies, where no physical sputtering is expected, carbon erosion yields comparable to those due to physical sputtering are observed [35–42]. This phenomenon has been under intense investigations during the recent years, as it is very relevant to detached divertor plasmas (T_e < 5 eV) with ion impact energies below $\sim$ 25 eV.

Analytical formulae for sputtering have been presented in the literature [43, 44], with empirical improvements to take into consideration the latest data on the chemical erosion of carbon [8, 33, 45]. These models depend highly on the understanding of the different erosion mechanisms and their extrapolation to lower energies has not always been successful.

Controlled laboratory experiments can provide information on the basic mechanisms of erosion, but cannot reach the high ion flux densities present in tokamaks and plasma simulators. The impact energies used in ion beam investigations are also too high in comparison with divertor plasmas, and data on carbon erosion by tritium is extremely scarce. On the other hand, the rapid development of computational tools and atomistic force models has offered an alternative way of studying carbon erosion mechanisms.

4.1 Physical sputtering and radiation enhanced sublimation

Physical sputtering is the ejection of atoms from a material surface under irradiation, due to momentum transfer between the projectile and the target atoms [46]. The sputtering process for a given projectile-target combination is characterized by a threshold energy (for hydrogenic ions on graphite $\sim$ 30 eV), below which no physical sputtering takes place. This energy is closely related to the binding energy of the target atoms at the surface, but also depends on the angle of incidence of the irradiation. The energy transferred from the projectile to the target atoms in elastic collisions is proportional to the kinematic factor $4M_1M_2/(M_1 + M_2)^2$, where M_1 and M_2 are the masses of the colliding atoms

[47]. Hence, in the case of hydrogen irradiation of materials, a strong ion isotope dependence of the sputtering is expected.

Analytical formulae for calculating physical sputtering yields were presented by Bohdansky [43], with revisions and improvements given later by García-Rosales *et al.* [44].

The physical sputtering yield does not depend on the target temperature. However, there exists another closely related, temperature-dependent erosion mechanism that has been observed only for carbon-based materials. Energetic irradiation of graphite creates Frenkel pairs (*i.e.* pairs of an interstitial atom and a vacancy site) in collision cascades in the lattice. The produced interstitials are known to migrate quite readily between the basal planes of graphite [48–50]. Upon reaching the surface, the interstitials can be thermally desorbed, as they have low surface binding energies of less than 1 eV. This process is called radiation enhanced sublimation (RES). At low temperatures Frenkel pair recombinations suppress the carbon emission. However, at $T > 1200$ K vacancies become mobile and can annihilate with native defects (*e.g.* plane edges). This results in an excess of interstitials and, subsequently, significant RES. Contrary to ordinary thermal sublimation, which becomes significant at ~ 2000 K, mostly monoatomic carbon is ejected from the surface.

4.2 Chemical erosion

The dominant erosion mechanisms of carbon at low plasma temperatures, and hence, low ion impact energies, can all be classified as chemical erosion. This entails the processes where the formation and breaking of chemical bonds are crucial for the erosion, leading to the ejection of molecular species from the surface. Along with the chemical erosion by hydrogen, carbon PFCs are very efficiently eroded by oxygen (C/O $\sim$ 0.1–1), with the formation of carbon oxides [51–54]. While the effect of oxygen can be suppressed with a selection of good gettering materials in the first wall, the intense flux of low-energy hydrogen is always present.

The nomenclature for different chemical erosion processes is by no means unambiguous. Scientists in different fields often use the terms chemical erosion, chemical sputtering, and etching for the description of similar processes. The latter term is seldom used in irradiation physics, and may be defined as the chemical erosion caused by thermal species, either in the liquid or gas phase.

Vietzke and Haasz define *chemical sputtering* as an erosion process involving at least one type of energetic species, reactive or inert [55]. However, the term 'energetic' is still vague, as it could mean energies in the keV, or just as well in the electronvolt range. The definition could be clarified by

stating that in order to call an erosion process chemical sputtering, the process should have an energy threshold where the yield drops to zero at some energy higher than thermal energies [56].

4.2.1 Chemical erosion by thermal hydrogen

Erosion of carbon by a flux of thermal hydrogen can occur via two known mechanisms, which are both initiated by the hydrogenation of unsaturated carbon atoms at the surface and at the edges of the graphite planes. The understanding of these mechanisms is in large extent due to the detailed studies by Küppers *et al.* [57–61] on interactions between ion beam deposited C:H layers and a hydrogen flux.

The first mechanism is simply the thermal ejection of surface hydrocarbon groups. These are formed due to an efficient hydrogenation by the thermal H flux. The rate limiting step for the erosion is the bond rupture between the surface carbon network and an sp^3-bonded CH_3 group. This is due to the fact that in a C:H system only the covalent C–C bonds, of which the sp^3 bond is the weakest, can strongly bind carbon atoms to the bulk. The activation energies for this process were determined to correspond to a 0.4 eV wide Gaussian distribution, centered at 2.4 eV [57]. The distribution, instead of a single activation energy, arises from the inhomogeneity of the bonding configuration in amorphous carbon networks.

The second, more complex mechanism was described in detail by Horn *et al.* [61]. The first step of the mechanism is the hydrogenation of an sp^2 carbon site, neighbouring another sp^2 site. The change in the bonding hybridization ($sp^2 \rightarrow sp^3$) forces the other site to adapt an intermediate, radical configuration sp^x. The key step in the erosion mechanism is the de-excitation of the sp^x carbon site with the split-off of a C(sp^3)–CH_x bond, with an activation energy of 1.6 eV.

The split-off mechanism described by Horn *et al.* is limited to a certain surface temperature range. At low temperatures the hydrogenation and dehydrogenation of carbon sites are the dominating processes. The erosion commences only at temperatures above $\sim$ 400 K, with appreciable rates of the sp^x site decomposition. The erosion rate increases with increasing temperature, peaking around 550 – 600 K at low H flux densities. At higher temperatures the breaking of C–H bonds starts to dehydrogenate surface carbon sites and suppresses the formation of sp^x sites. On the other hand, for high hydrogen fluxes obtained in plasma simulators, the peak temperature of the hydrocarbon erosion shifts to higher temperatures with increasing flux density [62], up to a limiting temperature of about 950 K.

Mainly CH_3 and CH_4 are ejected from the surface, but a wide distribution of heavier hydrocarbons (C_yH_x; $y \geq 2$) is also observed [55, 63]. The erosion yields depend on the type of the carbon structure used. Amorphous C:H samples result in much higher yields (up to ~ 0.1) than ordered networks, *e.g.* graphite. For *a*-C:H samples the hydrogenation occurs readily, as there are plenty of H bonding sites available. However, for different types of graphite, irradiation by energetic ions [55, 64, 65] is usually required in order to produce enough bonding sites for the impinging hydrogen flux. In the case of irradiation by energetic (> 50 eV) hydrogen, chemical erosion of carbon via hydrocarbon formation at the end of the ion range is also observed. The underlying mechanisms of erosion by the thermalized ions in the damaged lattice are presumed to be the same as described above [55].

4.2.2 Chemical sputtering by low-energy ions

It has been observed that carbon sputtering occurs at hydrogen irradiation energies far too small (~ 5 – 30 eV) to lead to appreciable physical sputtering [35–42]. There is comprehensive evidence of an isotopic effect on the carbon sputtering yield [39, 40], indicating a collisional process of some sort. As in the case of irradiation by thermal hydrogen, a temperature dependence of the sputtering yield is also observed. The peak temperature is at ~ 600 – 900 K [38–40] and decreases with ion energy. However, sputtering yields of the order of percents are observed even at 300 K, which excludes thermal erosion of the samples. No explanation for the temperature dependence of the hyperthermal ion irradiation has yet been given.

It was suggested by Roth and Bohdansky [35], that the erosion mechanism could be a chemically enhanced physical sputtering process, resulting from the surface hydrogenation and, consequently, formation of weakly bound surface hydrocarbon groups. The erosion process could then be a simple knock-on sputtering process, with a threshold energy much lower than for the case of pure graphite. While the weakly bound surface hydrocarbon groups are likely to play a role in this mechanism, the exact erosion mechanism has not been elucidated in the literature. Some knowledge has been provided by the empirical models for carbon sputtering [8, 45], which were fitted on sets of measured data. Yet, there is significant scatter in the experimental low-energy sputtering yield data [35, 36, 38–42]. The predictions of the models may only describe well the materials and conditions for which the data used for the fitting was measured.

The scatter in the experimental data could be partly due to different measurement methods. The distribution of the species eroded by the irradiation is a wide range of both saturated molecules and radicals. The latter can stick quite efficiently to measurement vessel walls [40], resulting in too low erosion yields by mass spectrometry analysis. Also, the use of molecular projectiles H_2^+/D_2^+ and H_3^+/D_3^+ for the low-energy sputtering yield measurements may also affect the results. It is generally

assumed that the projectile fragmentates to atoms that each have an equal fraction of the total kinetic energy of the projectile. This may not be the case at kinetic energies comparable to the bond energies of the projectile atoms.

4.3 Doping of carbon materials

The reduction of the chemical erosion of carbon is critical for its applicability as a PFC material. By introducing small amounts (several at.%) of impurities, the formation of non-volatile oxides and suppression of the hydrocarbon formation is desired. On the other hand, the excellent thermomechanical properties of carbon materials should not be degraded significantly by the dopants. In the case of amorphous carbon, some dopants may in fact act as catalysts for graphitization, thus improving the thermal properties of the sample [66]. In general, the best results are obtained with homogeneous or fine-grain distribution of dopants.

A vast amount of studies has been carried out on Si, B, Ti, V, and W, and their carbides, as dopants in different types of graphites and CFCs [66–68]. Generally, the carbon erosion yields of doped materials are decreased at least by a factor of two, compared with undoped carbon. For the low-energy hydrogen irradiation of doped materials, a surface enrichment of dopants is usually observed due to higher threshold energies of physical sputtering and low, or non-existent, chemical sputtering. This results in topographical changes in the surface microstructures, where the regions more susceptible to erosion are shielded by the dopant grains. For Ti-doped graphites, a reduction of the chemical sputtering yield by an order of magnitude with increasing fluence has been reported [36].

Experiments with Si-doped (up to 10 at.%) carbon materials have resulted in excellent overall plasma-facing properties [5, 69]. The chemical erosion of Si-doped graphites and CFCs is generally reduced by a factor of $2 - 3$ [27, 36, 70], while the formation of non-volatile SiO_2 layers reduces the carbon erosion by oxygen. As silicon has a moderately low atomic number, eroded Si impurities can still be tolerated in the fusion plasma up to some extent. Also, the thermal properties of Si-doped carbon structures are comparable to those of undoped carbon.

The reasons for the reduced carbon sputtering yields by Si-doping have not been thoroughly resolved. Although a surface enrichment of dopant grains, similar to the one obtained with metallic dopants, was observed at high doses of 20-eV deuterium irradiation [36], the carbon sputtering yield remained roughly constant throughout the experiment.

5 SIMULATION METHOD

Modeling studies can provide valuable insight on the ion-surface interactions of carbon irradiation by low-energy hydrogen. At energies below the regime of physical sputtering, it is clear that the methods used have to provide a realistic description of the intricate C–H chemistry. This rules out the use of programs based on the binary collision approximation (BCA) [71], which are otherwise widely used for simulating high-energy irradiation of materials.

There are no modeling studies in the literature on the sputtering mechanism of carbon by hyperthermal hydrogen. The mechanism was investigated in this thesis by the use of the molecular dynamics (MD) simulation method [72, 73]. For the most part, the modeling was concentrated on calculations of reliable sputtering yields with the empirical Brenner-Beardmore force model [74, 75]. However, in order to verify the sputtering mechanism described in paper **I**, and to study the possibility of quantum-mechanical effects on the sputtering process, calculations with a small system of atoms were also carried out with the tight-binding formulation by Porezag *et al.* [76, 77] in paper **II**.

5.1 Molecular dynamics

The molecular dynamics method is a formidable tool for studying processes on the atomic scale. Especially for studies of far-from-equilibrium processes, such as atomic cascades resulting from ion irradiation, where the applicability of analytic methods is sometimes questionable, MD simulations can provide valuable insight. After the first implementation of the method in the late 50's [78], the accuracy and speed of MD simulations have tremendously increased with the rapid development of the computer CPU speed and memory.

In molecular dynamics the motion of an ensemble of atoms is followed by solving the equations of motion for each atom [72, 73]. By deriving the velocities of the atoms from some force model, the evolution of the system is determined over a short time interval. However, in order to avoid a violation of the energy conservation or other spurious effects, the time step has to be kept sufficiently small, typically of the order of ~ 1 fs. This practically limits the maximum simulation time achievable to nanosecond time scales. Especially in simulations involving energetic particles, too abrupt changes in the atom positions may lead to unphysical behaviour. For the best computational efficiency in the calculations, a variable time step length may be used [79].

The MD methods can be crudely divided into two categories, classical and quantum-mechanical, depending on the force model used. In classical MD the interatomic forces are derived from some potential energy function. The parameters in the potential functions are taken either from *ab initio*

quantum-mechanical calculations or experimental data, such as the melting point, elastic constants, bond lengths and energies. Electronic effects are not included in the classical MD, and hence, all interatomic collisions are elastic.

The advantage of the classical models is their speed, as the computational time is linearly proportional to the number of atoms in the simulation. A typical system size with the classical MD is of the order of 10^3 – 10^6 atoms. Non-local effects, which take into consideration the bonding structure further away than the nearest neighbouring atoms, may be included in the potential to improve the accuracy of the calculations. This is especially important in the case of carbon, where heterogenous bonding configurations arise from the presence of sp^2- and sp^3-hybridized bonding.

The quantum-mechanical models range from computationally intensive *ab initio* to semi-empirical methods. The energy of a system of atoms is calculated by numerically solving the Schrödinger equation, with some approximations. While the calculations are physically better motivated than in the classical models, they are also computationally extremely demanding. Hence, the size of the system studied is usually restricted to ~ 2 – 100 atoms.

5.2 Brenner empirical hydrocarbon potential

The reactive bond order C–H potential developed by Brenner [74] was used in all the papers of this thesis. The potential is a modified Tersoff-type potential [80, 81], augmented with continuous bond-order correction functions. The parameters in the correction functions were fitted to a large number of experimental data for bulk carbon structures and small hydrocarbon molecules [74]. Beardmore and Smith later combined the Brenner potential with formulations for Si–C [82] and Si–H [83] interactions to a hybrid potential for Si-C-H systems [75].

As the interatomic forces in covalently bonded materials weaken rapidly with increasing distance, the calculations are sped up by imposing a maximum interaction distance (cutoff radius) for each combination of atom types in the simulation. All atoms outside the cutoff radius are neglected when calculating the force affecting a given atom.

The Brenner potential has a reasonably realistic description of pure carbon and hydrocarbon molecule structures, as well as dynamic effects, such as bond forming and breaking. Hence, it has been used for various studies of carbon and hydrocarbon systems [84–88]. However, some problems with the potential have been found. First, the structures given by the potential for dense amorphous carbon have been shown to contain too small fractions of sp^3–bonded carbon [89]. In paper **II** of this thesis it was observed that the chemical sputtering of carbon (at least from the very surface) was dependent

on the C–C interaction range of the potential. Also, the sticking probabilities of methyl radicals on unsaturated carbon sites have been shown to be much lower than those given by tight-binding calculations and experiments [88]. The last case is especially concerning, as the potential was originally formulated for the modeling of chemical vapor deposition growth of diamond.

However, it was shown in all the cases above that the results of the modeling could be improved by increasing the maximum C–C interaction range of the potential. It should be noted that the choice of the C–C cutoff radius in the original Tersoff formulation [80, 81] was somewhat arbitrary, but was later optimized by Nordlund *et al.* [90].

5.3 Tight-binding method

The tight-binding (TB) method [91] is a minimal quantum-mechanical method. It is based on the assumption that the total energy in an atomic system can be approximated as the sum of two terms: repulsive pair-wise interatomic potential, which gives the contribution of the core electrons of atoms, and the energy of the valence electrons. The former term is usually fitted to experimental data, making the method in fact semi-empirical. The latter term is calculated by solving the Schrödinger equation for electrons in the field of the atom cores, with the Hamiltonian replaced with a parametrized matrix. A set of basis functions, usually having the same symmetry properties as the atomic orbitals, is then used to describe the valence electron states.

The method has been shown to give a qualitatively correct description of various covalently bonded materials, and especially in view of this thesis, amorphous carbon [92, 93]. Also, the method is quite fast, compared with *ab initio* methods, allowing the study of larger systems and collecting at least moderate statistics for atomistic processes. While the carbon sputtering yields by low-energy hydrogen are still too low for comprehensive sputtering studies with the TB method, the quantum-mechanical treatment can still give a physically more accurate description of the chemical bond breaking than the classical methods.

In paper **II**, the tight-binding formulation by Porezag *et al.* [76, 77] was used for the irradiation simulations. The method differs from most TB formulations in the sense that it does not contain experimental parameters, but has been parametrized with results from *ab initio* calculations.

5.4 Modeling of the carbon bombardment by hydrogen

The hydrogen bombardment simulations were carried out with the HCPARCAS simulation code, developed by Nordlund at the Accelerator Laboratory. The program is especially tailored to simulate far-from-equilibrium phenomena, such as cascades produced by ion irradiation.

5.4.1 Simulation cells

Since the carbon PFC surfaces under intense hydrogen irradiation eventually amorphize, in all the studies of this thesis we used random C:H networks, consisting of 200 – 2000 atoms. The structures were optimized with pressure scaling and annealing simulations using the methods by Berendsen *et al.* [94], with periodic boundaries employed in all directions. After relaxing the structure at a given temperature, the periodic boundaries were removed in one direction. Atoms within 2 – 3 Å from the side of the cell opposite to the chosen surface were held fixed and the structure was relaxed for several tens of picoseconds to form a stable surface. The majority of the carbon atoms in the simulation cells were either threefold- or fourfold-coordinated, with some contributions from twofold-coordinated atoms at the surface. Although not every bonding configuration corresponded to an ideal hybridization geometry, the terms sp^2 and sp^3 will be used here for all the threefold- and fourfold-coordinated carbon sites, respectively. All hydrogen isotopes (H, D and T) were used in this study, both as impinging ions as well as atoms in the irradiated sample.

We mainly considered sample irradiation at 300 K, where no thermal erosion is expected. Typically, a hydrogen concentration corresponding to the bulk saturation H/C ratio of 0.4 (at 300 K) [95, 96] was chosen. However, in paper **IV** we also used temperature-dependent H/C saturation values [96, 97]. In paper **V** silicon was added in the C:H network in order to study the effect of doping on the chemical sputtering.

5.4.2 Bombardment simulation types

Although the term 'ion' is used here to distinguish the incident atom from the target atoms, the classical MD simulations do not describe the charge transfer reactions between the atoms. Thus, all the impinging atoms were in fact neutrals. This is not a major restriction for the modeling, as the ions impinging on the divertor plates in tokamaks will be promptly neutralized by the excess electrons at the surfaces.

In the series of impact simulations the impinging hydrogen ions were assigned either fixed kinetic energies or random energies according to a Maxwellian distribution, characterized by a root-mean-square energy E_{rms}. The former approach allowed the study of the chemical sputtering as a function energy and was better suited for comparisons with laboratory experiments, where almost monoenergetic ion beams are used. The latter case corresponds better to hydrogen bombardment of carbon PFCs in tokamaks, where the incident energies follow approximately Maxwellian distributions.

We carried out two types of irradiation simulations: cumulative and non-cumulative. The non-cumulative simulations used the same initial surface for all the impact events in a series of simulations and thus concentrated on probabilities of surface processes. The cumulative simulations allowed to study the effect of the irradiation on the surface structure, as the surface produced in an impact event was used as the target for the next impact event. These simulations generally require larger cells, as part of the surface layer is eroded away during the hydrogen irradiation, making the calculations more time-consuming. While the cumulative simulations may seem more realistic, it should be noted that computational limitations restrict this approach to simulations of extremely high irradiation flux densities. An ion impact every 2 – 3 picoseconds on a simulation cell surface area typically used in our modeling ($\sim 20 \times 20$ Å^2) corresponds to an irradiation flux density of about 10^{29} m^{-2}s^{-1}. This is five orders of magnitude higher than will be reached in ITER.

5.4.3 Effect of the amorphous surface structure

In simulations of a crystalline sample irradiation the impact points are usually chosen inside a small area on the surface due to symmetry. However, this cannot be done for amorphous structures. Hence, before each impact event the simulation cell was shifted at random in the plane perpendicular to the surface normal so that the whole surface could be used as a target for the hydrogen bombardment.

During the course of this study it became evident that quantitative comparisons of the sputtering yields obtained for structures with different Si concentrations could be influenced by differences in the cell surface microstructures. Thus, in order to obtain reliable sputtering yield statistics, several surfaces were used for each Si concentration. It is then relevant to ask, whether this effect could influence the results of the previous studies as well. However, most of our studies concentrated on various trends (*e.g.* energy, isotope or temperature dependence) of the carbon sputtering yield. As the results for different simulation cells in these cases were qualitatively similar, it can be stated that the surface microstructure did not have a significant effect on the main conclusions of any part of our work.

6 RESULTS

The main finding of this thesis is a chemical sputtering mechanism of carbon by low-energy (≤ 35 eV) hydrogenic species. Although experiments have not produced a clear picture of how the sputtering of carbon by low-energy hydrogen takes place, our modeling provides a detailed description of the sputtering mechanism and explains the observed isotopic effect. The mechanism was further verified with more sophisticated tight-binding simulations. In this section the results of our modeling are summarized. The sputtering mechanism and its energy dependence are first described, followed by studies on the effects of the surface temperature, ion irradiation flux, and Si doping on the carbon sputtering yield.

6.1 Swift chemical sputtering mechanism

The main erosion mechanism of carbon in our modeling was a process we call *swift chemical sputtering*. This mechanism and its energetics were first presented in paper **I**, and were further studied in papers **II** and **IV**. The term 'swift' is used since the process of bond breaking, and subsequent erosion, usually takes place during the first 500 fs of the impact simulation. On the other hand, the mechanism is 'chemical sputtering' in the sense that it requires energetic particles and the key factor in the sputtering process is the breaking of covalent C–C bonds by the projectile. Furthermore, in some cases the bond breaking was enhanced by the bonding of the ion to one of the surface atoms.

The sputtering mechanism can be described as follows. A hydrogenic ion attacks the region roughly between two carbon atoms. Provided the ion is energetic enough, this results in core–core repulsion between the ion and the carbon atoms. At short interatomic distances the repulsive interaction efficiently pushes the two carbon atoms apart from each other and the covalent C–C bond is broken. The carbon atoms that had formed the ruptured bond obtain finite momenta, and provided one of them is no longer bound to the bulk network, ejection of carbon atoms or hydrocarbon species can occur (see Fig. 5). As H–C bonds are only terminating bonds, it is the number of the C–C bonds (and Si–C bonds if Si is included in the bulk network) that determines how easily a carbon atom is sputtered from the surface.

If the energy of the ion is too low, it is repelled by the core–core repulsion before it breaks the bond. In that case the collision leads only to small momentum transfer from the ion to the carbon atoms. Furthermore, if the energy of the ion is too high, the ion passes between the carbon atoms too quickly for bond breaking. The effect of the incident ion energy on the momentum transfer is illustrated for the case of a H atom attacking a carbon dimer in Fig. 6. The figure shows the H–C potential energy,

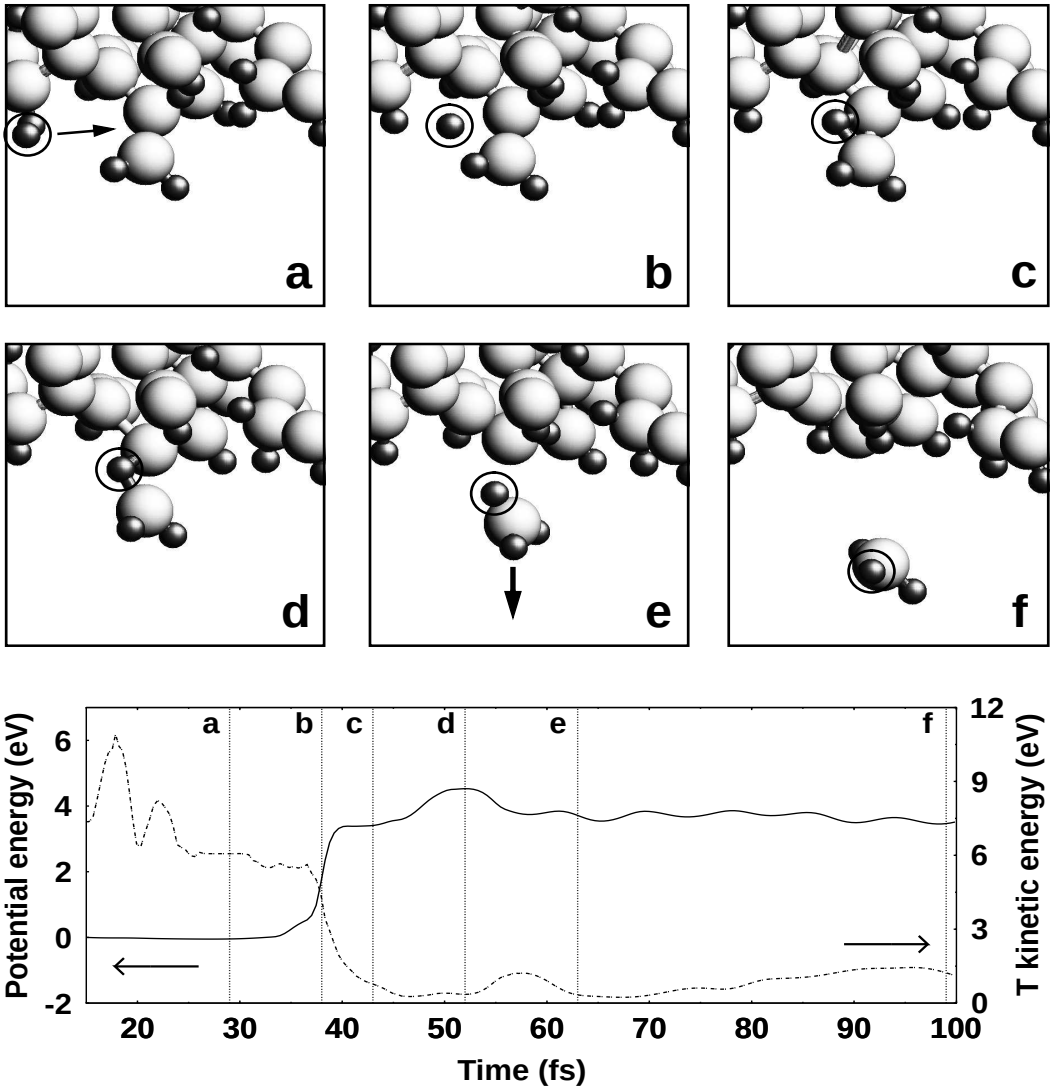

Figure 5: Hydrocarbon sputtering from an *a*-C:T surface by an impinging T ion (circled). The light spheres represent C atoms and the dark ones T atoms. In the first frame (a) we see the ion approaching a CT_2 group at the surface. The initial velocity direction of the ion is designated with the arrow. The ion penetrates between two carbon atoms (b) – (d), forces them apart and bonds to the carbon atom leaving the surface. The CT_3 group has a finite velocity away from the surface (e) and is sputtered (f). The graph below shows the potential energy of the system (with zero corresponding to the initial potential energy). The letters (a) – (f) in the graph refer to the snapshots above. It is seen that the potential energy of the system is raised by about 4 – 5 eV during the bond breaking process. From Ref. [56].

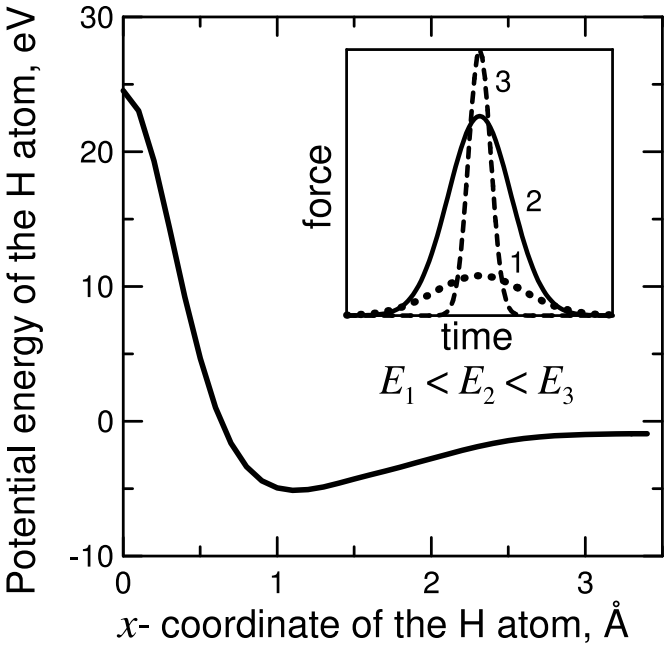

Figure 6: Potential energy of a H atom as a function of the distance x from the midpoint between the atoms of a carbon dimer. The inset schematically shows the force affecting the carbon atoms as a function of time as the ion traverses the region between them. From paper **II**.

with repulsive (positive) values at H–C distances smaller than ~ 0.6 Å. The inset shows the core–core repulsion as a function of time for three different incident energies, as the H atom passes between the carbon atoms. The total momentum transferred to the carbon atoms is the integral of the force over time.

The momentum transfer explains the observed isotope effect [39, 40] of the low-energy sputtering yields. For two hydrogenic ions with the same energy but different masses, the heavier isotope has a lower velocity. Thus, the time during which the core–core repulsion is effective, and consequently the total momentum transferred, is increased for ions of heavier masses. The energy required for the bond breaking is still the same in both cases.

Fig. 7 illustrates the necessity of the hydrogenic ion attacking the region between the carbon atoms. As a model system, a C_2D_4 molecule is irradiated by 20-eV D ions, perpendicularly to the line joining the two carbon atoms. The points where the ion would impact according to its original position have been plotted in the figure. It is seen that only impact points in the region between the carbon atoms lead to bond rupture. The wide distribution of these points in the y-direction is due to the attractive C–D interaction at larger distances, turning the impinging ion slightly towards the carbon atoms. Note also that impacts on the carbon atoms, analogous to the knock-on processes of physical sputtering do *not* lead to bond breaking.

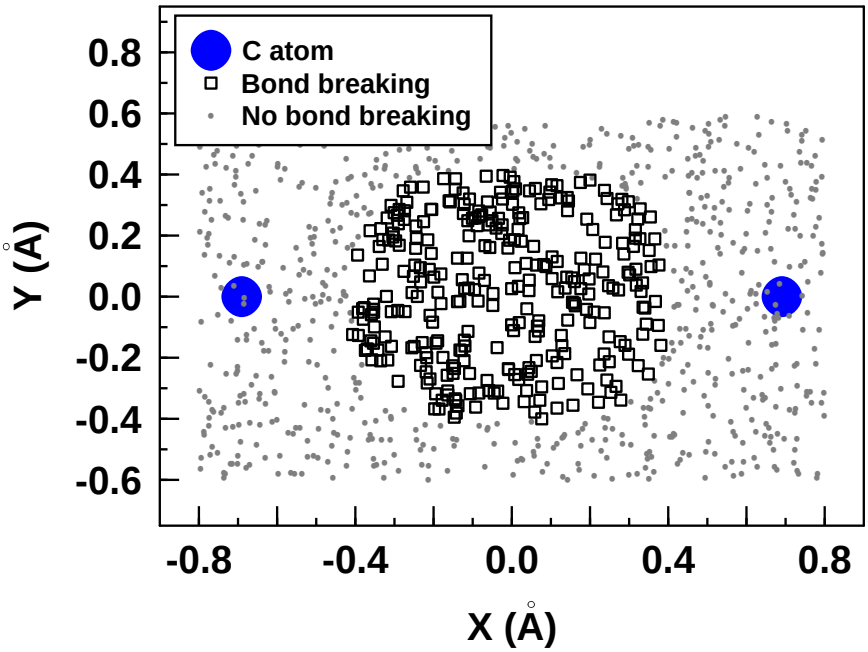

Figure 7: Illustration of the impact point dependence of the swift chemical sputtering mechanism. A C_2D_4 molecule has been bombarded with 20-eV D ions, with random impact points parallel to the line joining the two carbon atoms. The open squares indicate impact points where bond breaking took place upon impact. The small dots designate impact points with no bond breaking.

In all of our studies, the eroded species were mainly small CH_x (x = 0, 1, 2, 3, 4) and C_2H_y (y = 1, 2, 3, 4, 5, 6) hydrocarbons, with significant contributions from radical species. (The chemical symbol H is used here for all the hydrogen isotopes.) This is in qualitative agreement with experimental results where the carbon sputtering is also dominated by small hydrocarbon species [38, 39, 41]. As an example, Fig. 8 shows mass distributions of eroded species for incident ion energies 5 – 30 eV, averaged over several simulation cell surfaces.

6.2 Energy dependence of the chemical sputtering

Sputtering by the swift chemical bond breaking is clearly dependent on the incident ion energy, as a single bond breaking event consumes an energy of several eV's. As the ion also loses energy in collisions with the surface atoms, it can be expected that the carbon sputtering yields drop sharply at energies lower than $\sim$ 10 eV. Generally, no carbon sputtering was seen at impact energies below 5 eV. However, by further studying impact events where carbon sputtering took place, and gradually lowering the ion energy while still retaining all the other impact parameters, bond breaking could still be observed with ion energies as low as $\sim$ 1 eV. In some cases chemical reactions, similar to the nucleophilic substitution reported by Garrison and Goddard [99] for Si etching by F, were observed. These events were still extremely rare and did not contribute significantly to the carbon sputtering.

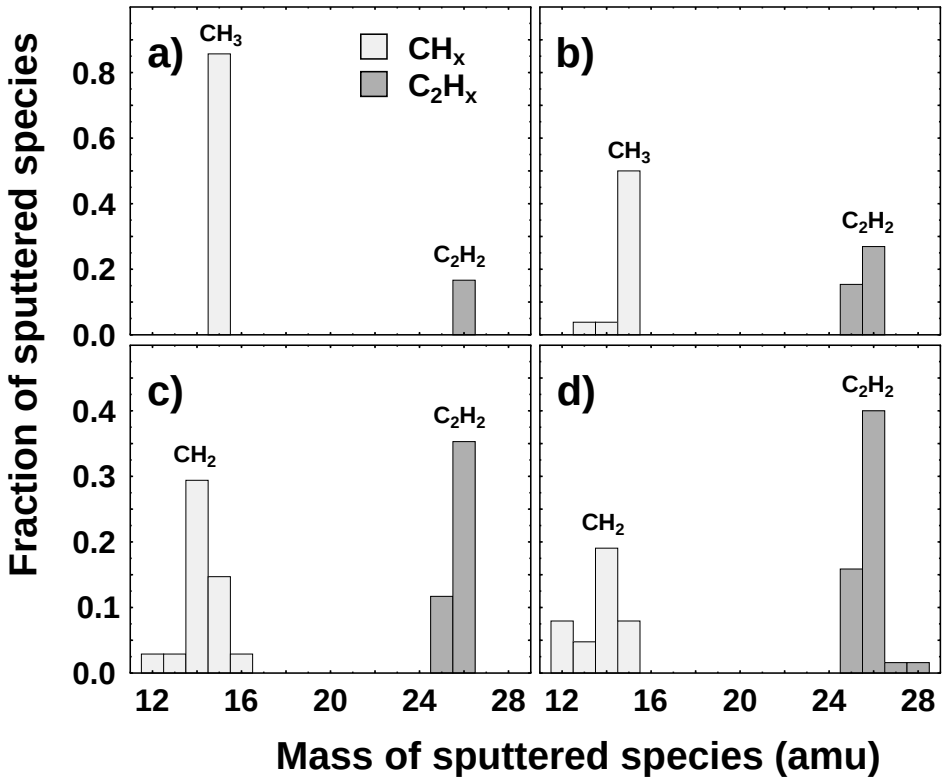

Figure 8: Mass distributions of sputtered hydrocarbon species for incident H energies of (a) 5, (b) 10, (c) 20, and (d) 30 eV. The scatter in types of eroded species at lower (5 and 10 eV) energies is due to the small number of sputtered hydrocarbons. From Ref. [98].

Higher ion energies, on the other hand, may lead to multiple scattering and bond breaking in the top surface layers. This increases the sputtering yield, but the effect is limited to energies, where the ion deposits most of its kinetic energy right at the surface. In many cases the carbon sputtering yield was observed to slightly peak around energies 15 – 25 eV.

The same sputtering mechanism was observed with both the empirical and tight-binding force model. This essentially verifies the mechanism, as the force models have very little in common. The discrepancies between the sputtering yields obtained in paper **II** and previous studies can be explained with much smaller simulation cells (due to the computational cost of the TB model), increased average carbon–carbon coordinations, and the low number of impact events, which could result in higher statistical uncertainties than the ones estimated in paper **II**. However, it was shown that a better agreement between the two models could be obtained with increasing the C–C cutoff radius of the Brenner model.

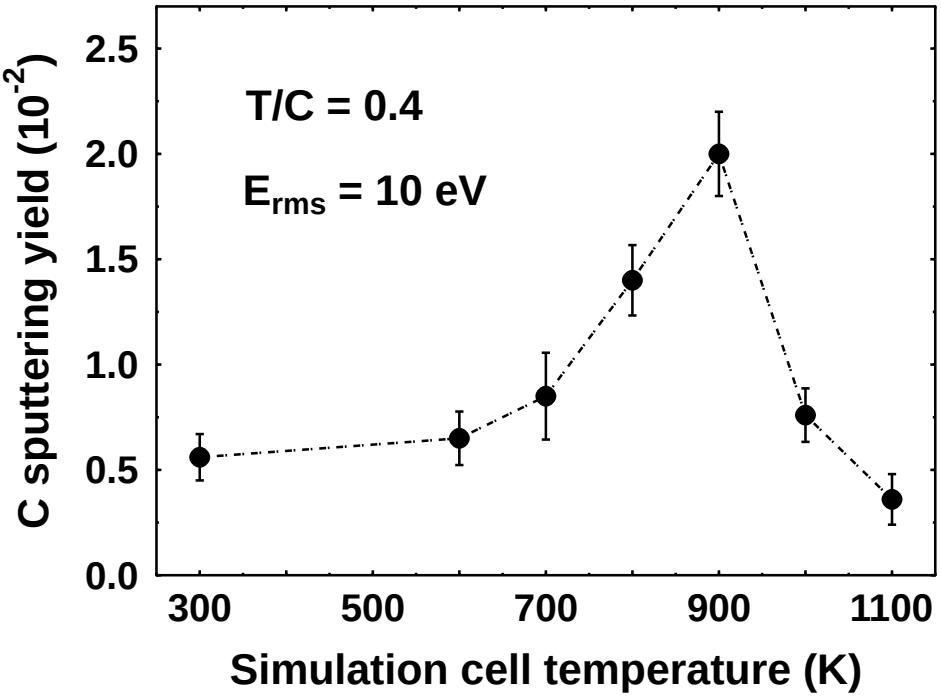

Figure 9: Carbon sputtering yield as a function of temperature for a typical simulation cell with a T/C ratio of 0.4. The root-mean-square energy of the impinging ions was 10 eV. From paper **I**.

6.3 Effect of temperature on the chemical sputtering

While a temperature dependence of the erosion yield is conventionally regarded as a sign of chemical erosion [100], the swift bond breaking process should not be strongly affected by the temperature of the irradiated surface. Yet the carbon sputtering yields obtained in simulations with slowly heated and subsequently relaxed cells were clearly temperature-dependent (papers **I** and **IV**), as observed in the experiments of the low-energy sputtering (see 4.2.2). This was obtained for all the simulation cells with a constant H/C ratio of 0.4 at temperatures between 300 and 1100 K. The peak temperature was typically around 800 – 900 K (see Fig. 9). No thermal desorption of surface hydrocarbon species was observed in our simulations.

The temperature dependence of the sputtering yields was concluded to result from changes in the bonding structures of the irradiated surfaces. It was observed that the fraction of sp^2 carbon atoms in the simulation cell increased with temperature, whereas the fraction of sp^3 atoms decreased. Thus, as the H/C ratio was kept constant throughout the temperature range of 300 – 1100 K, the average carbon–carbon coordination in the cell decreased with temperature. This increased the number of carbon atoms prone to chemical sputtering.

Since the increase of the fraction of threefold-coordinated carbon atoms in the simulation cells in-

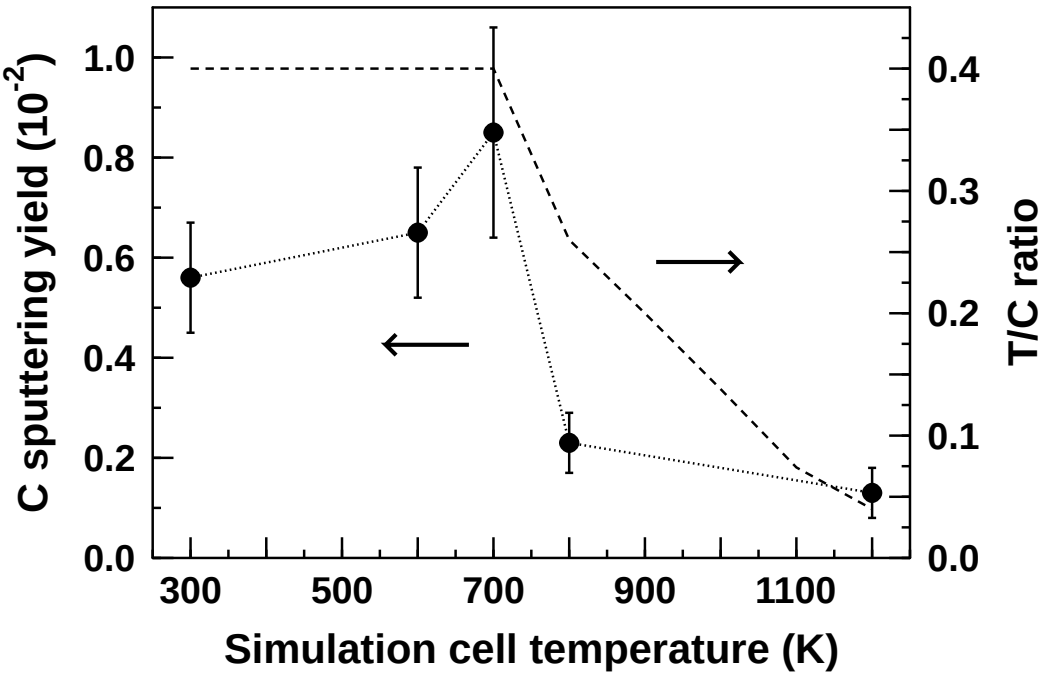

Figure 10: Temperature dependence of the carbon sputtering yield by tritium irradiation with E_{rms} = 10 eV. The T/C ratios were chosen according to the experimentally observed temperature-dependent hydrogen saturation concentrations, with irradiation taking place at the respective temperature. From paper **IV**.

creased monotonically, a competitive process is required for obtaining a peak temperature for the carbon sputtering yield. No temperature dependence of the sputtering yield was observed with rapidly heated cells where structural rearrangements had no time to take place. This shows that the effect of thermal vibrations was of secondary importance.

The depth distributions of the eroded species showed a trend toward the surface with increasing temperature. The effect was more pronounced at temperatures above 900 K, giving a first indication of an erosion-reducing process. This was studied in more detail with simulations in which a randomly chosen carbon atom in the cell was given a velocity toward the surface. The kinetic energy of the atom was chosen large enough to overcome its binding energy in the network. With the kinetic energy gradually increased, it was observed that at higher temperatures higher kinetic energies (in reference to the binding energies) were required, on average, to eject carbon atoms and hydrocarbon species from the surface. It was assumed that the unbound hydrocarbon species could rebond to carbon sites while traversing toward the surface. This effect would then become stronger with increasing temperature and the decrease of the average carbon atom coordination. The explanation seems plausible, as carbon favours both threefold- and fourfold-coordinated bonding configurations in the network, and is further strengthened by the observation of a similar rebonding effect in paper **V**.

However, while this investigation provided insight on the swift chemical sputtering mechanism, in reality the H/C saturation ratio in hard carbon structures is temperature dependent, as reported in Refs. [96, 97]. Thus, the temperature dependence of the carbon sputtering yield was also calculated for C:H networks with realistic hydrogen saturation concentrations. We considered both samples which had been irradiated at the respective temperature and samples which had been first hydrogenated and then heated (see paper **IV**).

The first case is probably closer to the case in fusion devices with elevated divertor target plate temperatures, as the hydrogenation of the carbon PFCs occurs very quickly. As can be seen from Fig. 10, there is only a weak sputtering yield maximum at 700 K for this case, after which the yield drops significantly with increasing temperature. The explanation here is simpler than in the case of a constant H/C ratio. The hydrogen concentration remains somewhat constant up to the peak temperature, and the increase in yield is explained with the increase of threefold-coordinated carbon atoms. However, at higher temperatures the H/C ratio drops quite rapidly, and while the average carbon coordination remains above three, the average number of carbon-carbon bonds per C atom increases. As the breaking of the C–C bonds is the critical step for the erosion, the sputtering yield is then suppressed.

6.4 High-flux hydrogen irradiation

The effect of high-flux hydrogen bombardment on the chemical sputtering of carbon was studied in papers **III** and **IV**. As the ion energies decrease at higher flux densities (due to the decrease of T_e), we chose Maxwellian energy distributions with root-mean-square energies (E_{rms}) of 1 and 10 eV. Cumulative simulations showed that the number of hydrogen atoms in the cells increased rapidly during the first 500 – 1000 impact events (cf. Fig. 11), and eventually reached a steady-state. The small increments after $\sim$ 2000 impact events were due to replacement collisions, driving surface hydrogen atoms deeper in the cell.

The H/C ratios in the simulation cells were clearly higher than the bulk saturation value of $\sim$ 0.4. Thus, the hydrogen concentration due to the high-flux bombardment was designated 'supersaturated'. Although incident ion reflection was the most frequent ion-surface interaction, the fraction of hydrogen capture to form H_2 molecules was much higher for the supersaturated surface than for the pristine one.

The carbon sputtering yields from the pristine surfaces were of the order of $\sim$ 0.01. However, for the supersaturated surfaces the yield was roughly an order of magnitude lower. The explanation for this effect is that the supersaturated hydrogen concentration at the surface efficiently shields the carbon

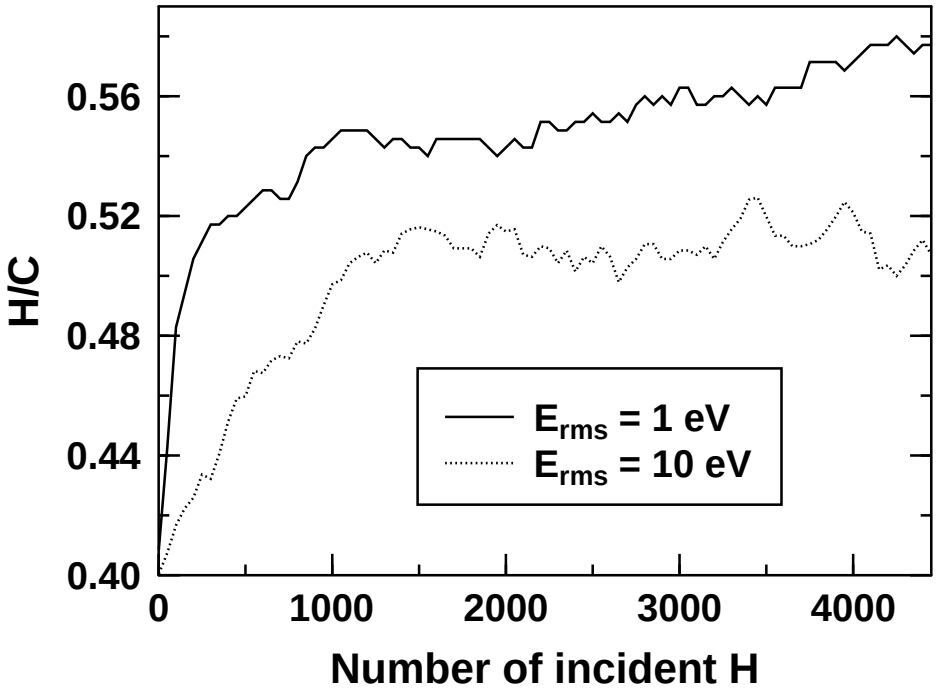

Figure 11: H/C ratios for *a*-C:H surfaces impinged on by H ions. The ion energies were according to Maxwellian distributions with root-mean-square energies of 1 (solid line) and 10 eV (dotted line). It is seen that the number of hydrogen atoms in the simulation cells initially increases rapidly. After about 2000 impact events the H/C ratios saturate to values above 0.5. From papers **III** and **IV**.

atoms in the network. As the incident ions had quite low energies, their ability for C–C bond breaking decreased on every collision with the surface H.

The supersaturated hydrogen concentration at the surface is a reasonable explanation for the flux dependence of the C erosion yield in tokamak and plasma simulator experiments (see 3.4.2). Whether the effect observed in experiments is due to the high flux density or low impact energies (as these are connected in divertor plasmas) is not important for our explanation. However, the critical factor is the stability of the supersaturated hydrogen concentration. The effect of the hydrogen shielding can be reduced due to: (1) hydrogen diffusion deeper into the C:H network; (2) thermal emission of hydrogen atoms and molecules (outgassing); or (3) H_2 formation due to hydrogen capture by the impinging ion.

The diffusion of the surface hydrogen into the bulk was determined to be negligible, based on the diffusion constants given in Ref. [101]. The probability for H_2 formation due to hydrogen capture was determined directly from the irradiation simulations. A probability of ~ 0.2 per incident ion was obtained for the supersaturated surfaces.

The thermal outgassing of the surface hydrogen was studied with simulations up to 1 ns at temperatures between 300 and 2400 K. An estimate for the outgassing rate at higher temperatures was

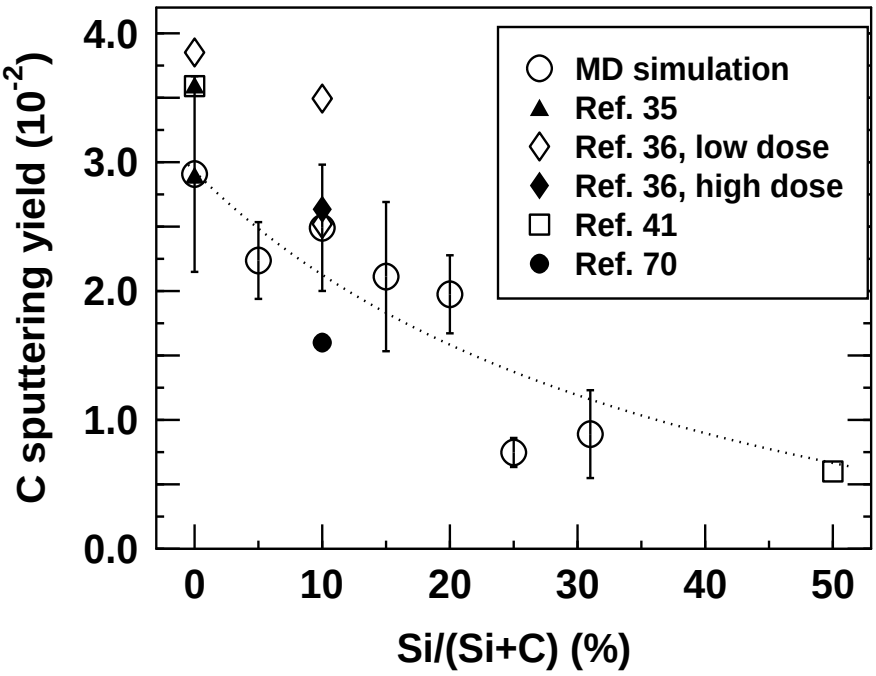

Figure 12: Sputtering yield of carbon as a function of the Si concentration. The line is a fit to our simulated data (open circles). Experimental data for graphite [35, 36, 41], 10 at.% Si-doped carbon [36, 70] and SiC [41] are also shown. From paper **V**.

obtained, but no hydrogen emission was seen at 300 K. However, this approach is somewhat limited as recombinations of surface hydrogen atoms, further apart from each other than the H–H cutoff radius of the Brenner potential, could affect the outgassing rates. To take this effect into consideration a potential energy function describing also weak long-range interactions, such as the AIREBO [102], is required, with a substantial cost of computational time. However, as no outgassing was observed in 1 ns simulations at 300 K, it can be estimated that the hydrogen supersaturation could still be obtained with flux densities at least as low as $\sim 10^{26}$ m^{-2}s^{-1}.

6.5 Effect of silicon doping on the carbon sputtering

In paper **V** the effect of silicon doping on the chemical sputtering of carbon was studied. We considered amorphous hydrogenated Si–C structures under 20-eV D irradiation. As the thermal properties of doped carbon structures generally become worse with increasing impurity concentrations, experiments have been carried out with silicon doping concentrations only up to Si/(Si+C) = 0.1 [36, 70]. Higher Si concentrations (up to Si/(Si+C) = 0.3) were used in our modeling to study the effect of the silicon concentration on the sputtering yields.

The results showed a decreasing trend of the carbon sputtering yield with increasing Si concentration (cf. Fig. 12). The obtained sputtering yields, as well as a fit to the simulated data to extrapolate our results to higher Si concentrations, were in good agreement with the experiments.

The reduced carbon sputtering yields were observed to result from the longer Si–C bond lengths, compared with the C–C bonds, and the dynamic rebonding of unbound hydrocarbon species (*i.e.* species whose C/Si bonds that bind them to the bulk network had been broken). The former reason was verified with a model system study, where the Si–C interaction range of the Brenner–Beardmore potential was shortened, while still preserving the equilibrium bonding characteristics. The dynamic rebonding was studied by analyzing in detail hundreds of bombardment events and further verifying the rebonding energetics to threefold- and fourfold-coordinated Si sites with the empirical potential and calculations based on the density functional theory [103].

The Si sputtering yields were at least an order of magnitude lower than the C sputtering yields, and much lower than expected simply from the concentrations of the Si atoms. This was due to the high number of C/Si bonds of the Si atoms and, in view of physical sputtering, a smaller maximum energy transfer coefficient (~ 0.25) for the impinging ion.

7 CONCLUSIONS AND OUTLOOK

In this thesis the chemical sputtering of carbon-based materials by hydrogen was studied under different irradiation conditions. The main merit of this thesis is in the qualitative description of the mechanism of carbon sputtering by hyperthermal atoms and the factors contributing to it. In the present-day tokamak divertors, with low T_e, the most important erosion process of carbon PFCs is the sputtering by hydrogenic species with energies below the threshold energy of physical sputtering. While it essentially determines the lifetime of the PFCs and plasma contamination by the eroded species, the exact erosion mechanism has not yet been known. All the knowledge of it has previously been based on fits to measured sputtering yield data with a wide scatter. Considering this, the verification of the swift chemical sputtering mechanism with two independent force models is most encouraging. Furthermore, the experimentally observed temperature and isotope dependencies of the low-energy sputtering are explained by our simulations.

For future simulations of the chemical sputtering of carbon, several factors will have to be taken into account. First, the Brenner empirical potential, although computationally the only method fast enough for comprehensive sputtering yield calculations, has shown to give results which are dependent on the cutoff radius of the model. The potential should be optimized for different systems by comparing

the calculations to more accurate methods, *e.g.* tight-binding. Second, for a better comparison of the results, a detailed knowledge of the surface microstructure of the samples used in experiments should be obtained. But most importantly, a stronger collaboration between the experimental and computational research needs to be established for the best efficiency in the development of the carbon PFC materials.

A current trend in the computational modeling of physical processes is to combine the accuracy of the quantum-mechanical models with the speed of the classical ones. The modeling can be further enhanced with cruder but much faster methods, such as Monte Carlo simulations, to achieve accurate results over time scales of up to seconds. This approach could prove quite useful for simulating the erosion of divertor materials in tokamaks, as several erosion mechanisms with different characteristic time scales are always present.

ACKNOWLEDGEMENTS

I wish to thank my supervisor Prof. Juhani Keinonen, head of the Department of Physical Sciences, for his guidance and comments during the course of this work. I thank Prof. Jyrki Räisänen and Doc. Eero Rauhala, the former and current heads of the Accelerator Laboratory, for placing the facilities of the laboratory at my disposal. I am also thankful to Prof. Kari Laasonen for his comments and criticism on this thesis.

I am deeply indebted to my supervisor Doc. Kai Nordlund for his guidance in the world of atomistic simulations and materials science in general. He has always had time for my questions and new ideas, and has patiently put up with my occasional moods of frustration.

Warm thanks are due to Prof. Chung Wu, who has been the driving force of our fusion-related materials research. I also thank Dr. Nino Runeberg for his valuable collaboration in our studies.

I am thankful to my co-workers at the Accelerator Laboratory for many fun moments, both in and outside the lab, and for creating a pleasant working atmosphere. I owe special thanks to Drs. Arkady Krasheninnikov, Jura Tarus, Kai Arstila, Tommy Ahlgren, and Timo Sajavaara, M.Sc, for many enlightening discussions.

I want to thank my family for their constant support and encouragement through the years. Finally, my warmest thanks are due to my girlfriend Pirita for all her love, understanding and unending patience.

Financial support from the Magnus Ehrnrooth foundation and the Vilho, Yrjö and Kalle Väisälä foundation is gratefully acknowledged.

Helsinki, June 2002

Emppu Salonen

REFERENCES

1. For further information on the scenarios of the World Energy Council on global energy consumption, energy resources and carbon emissions, see the WEC web site `http://www.worldenergy.org/wec-geis/`.

2. J. J. Brehm and W. J. Mullin, in *Introduction to the structure of matter* (John Wiley & Sons, New York, USA, 1989), Chap. 15.

3. More information on the fusion technology research and development can be found at the ITER web page, `http://www.iter.org/`.

4. G. Janeschitz and ITER JCT and HTs, *Plasma-wall interaction issues in ITER*, J. Nucl. Mater. **290-293**, 1 (2001).

5. C. H. Wu, C. Alessandrini, R. Moormann, M. Rubel, and B. M. U. Scherzer, *Evaluation of silicon doped CFCs for plasma facing material*, J. Nucl. Mater. **220-222**, 860 (1995).

6. V. Barabash, G. Federici, R. Matera, A. R. Raffray, and ITER Home Teams, *Armour materials for the ITER plasma facing components*, Physica Scripta **T81**, 74 (1999).

7. G. Federici, R. A. Anderl, P. Andrew, J. N. Brooks, R. A. Causey, J. P. Coad, D. Cowgill, R. P. Doerner, A. A. Haasz, G. Janeschitz, W. Jacob, G. R. Longhurst, R. Nygren, A. Peacock, M. A. Pick, V. Philipps, J. Roth, C. H. Skinner, and W. R. Wampler, *In-vessel tritium retention and removal in ITER*, J. Nucl. Mater. **266-269**, 14 (1999).

8. J. Roth, *Chemical erosion of carbon based materials in fusion devices*, J. Nucl. Mater. **266-269**, 51 (1999).

9. J. Winter, *Wall conditioning of fusion devices by reactive plasmas*, J. Nucl. Mater. **161**, 265 (1989).

10. J. Küppers, *The hydrogen surface chemistry of carbon as a plasma facing material*, Surf. Sci. Rep. **22**, 249 (1995).

11. R. Parker, G. Janeschitz, H. D. Pacher, D. Post, S. Chiocchio, G. Federici, P. Ladd, ITER Joint Team, and Home Teams, *Plasma-wall interactions in ITER*, J. Nucl. Mater. **241-243**, 1 (1997).

12. C. H. Wu and U. Mszanowski, *A comparison of lifetimes of beryllium, carbon, molybdenum and tungsten as divertor armour materials*, J. Nucl. Mater. **218**, 293 (1995).

13. W. H. Zhao, A. Koch, U. H. Bauder, and R. Behrisch, *First wall erosion by arcing*, J. Nucl. Mater. **128 & 129**, 613 (1984).

14. W. Wang, J. Roth, S. Lindig, and C. H. Wu, *Blister formation of tungsten due to ion bombardment*, J. Nucl. Mater. **299**, 124 (2001).

15. E. Hechtl, H. R. Yang, C. H. Wu, and W. Eckstein, *An experimental study of tungsten self sputtering*, J. Nucl. Mater. **176 & 177**, 874 (1990).

16. W. Eckstein and J. László, *Sputtering of tungsten and molybdenum*, J. Nucl. Mater. **183**, 19 (1991).

17. Y. Hirooka, *Review of beryllium and tungsten erosion behaviour and universal modeling of plasma impurity effects observed in recent PISCES experiments*, Physica Scripta **T64**, 84 (1996).

18. P. Andrew *et al.*, *Tritium recycling and retention in JET*, J. Nucl. Mater. **266-269**, 153 (1999).

19. The acronym is from Russian, meaning “toroidal chamber and magnetic coil”.

20. M. R. Wade *et al.*, *Impurity enrichment and radiative enhancement using induced SOL flow in DIII-D*, J. Nucl. Mater. **266-269**, 44 (1999).

21. D. G. Whyte, G. R. Tynan, R. P. Doerner, and J. N. Brooks, *Investigation of carbon chemical erosion with increasing plasma flux and density*, Nucl. Fusion **41**, 47 (2001).

22. ASDEX Upgrade web page, `http://www.aug.ipp.mpg.de/aug.eng/`.

23. *CRC Handbook of Chemistry and Physics, 76th ed.*, edited by D. R. Lide (CRC Press, Boca Raton, FL, USA, 1995).

24. V. Rohde, H. Maier, K. Krieger, R. Neu, J. Perchermaier, and the ASDEX Upgrade Team, *Carbon layers in the divertor of ASDEX Upgrade*, J. Nucl. Mater. **290-293**, 317 (2001).

25. J. Roth, *Synopsis of erosion and redeposition*, Physica Scripta **T 91**, 65 (2001).

26. A. Kallenbach, A. Thoma, A. Bard, K. Behringer, K. Schmidtmann, M. Weinclich, and the ASDEX upgrade team, *Evidence for hydrogen flux dependence of the apparent chemical erosion yield of graphite under high flux conditions*, Nucl. Fusion **38**, 1097 (1998).

27. H. Grote, W. Bohmeyer, P. Kornejew, H.-D. Reiner, G. Fussmann, R. Schlögl, G. Weinberg, and C. H. Wu, *Chemical sputtering yields of carbon based materials at high ion flux densities*, J. Nucl. Mater. **266-269**, 1059 (1999).

28. R. D. Monk, C. H. Amiss, H. Y. Guo, G. F. Matthews, G. M. McCracken, and M. F. Stamp, *The Behaviour of the Apparent Chemical Sputtering Yield in the JET Tokamak*, Physica Scripta **T81**, 54 (1999).

29. A. Kallenbach, A. Bard, D. Coster, R. Dux, C. Fuchs, J. Gafert, A. Herrmann, and R. Schneider, *New results on carbon release and transport in ASDEX-Upgrade*, J. Nucl. Mater. **266-269**, 343 (1999).

30. M. F. Stamp, S. K. Erents, W. Fundamenski, G. F. Matthews, and R. D. Monk, *Chemical erosion yields and photon efficiency measurements in the JET gas box divertor*, J. Nucl. Mater. **290-293**, 321 (2001).

31. A. Pospieszczyk, V. Philipps, E. Casarotto, U. Kögler, B. Schweer, B. Untenberg, and F. Weschenfelder, *Chemical erosion measurements from various carbon limiters and coatings in TEXTOR-94*, J. Nucl. Mater. **241-243**, 833 (1997).

32. A. Kallenbach, A. Bard, A. Carlson, R. Dux, and the ASDEX Upgrade Team, *Chemical erosion of carbon in the divertor of ASDEX Upgrade*, Physica Scripta **T81**, 43 (1999).

33. J. Roth and C. García-Rosales, *Analytic description of the chemical erosion of graphite by hydrogen ions*, Nuclear Fusion **36**, 1647 (1996), with corrigendum Nuclear Fusion **37**, 897 (1997).

34. W. Eckstein, *Physical sputtering and reflection processes in plasma-wall interactions*, J. Nucl. Mater. **248**, 1 (1997).

35. J. Roth and J. Bohdansky, *Sputtering of graphite with light ions at energies between 20 and 1000 eV*, Nucl. Instr. Meth. Phys. Res. **B23**, 549 (1987).

36. H. Plank, R. Schwörer, and J. Roth, *Surface composition modifications of carbides and doped graphites due to D^+ ion bombardment*, Surf. Coat. Technol. **83**, 93 (1996).

37. A. Annen and W. Jacob, *Chemical erosion of amorphous hydrogenated boron films*, Appl. Phys. Lett. **71**, 1326 (1997).

38. B. V. Mech, A. A. Haasz, and J. W. Davis, *Chemical erosion of pyrolytic graphite by low-energy H^+ and D^+ impact*, J. Nucl. Mater. **241-243**, 1147 (1997).

39. B. V. Mech, A. A. Haasz, and J. W. Davis, *Isotopic effects in hydrocarbon formation due to low-energy H^+/D^+ impact on graphite*, J. Nucl. Mater. **255**, 153 (1998).

40. M. Balden and J. Roth, *New weight-loss measurements of the chemical erosion yields of carbon materials under hydrogen ion bombardment*, J. Nucl. Mater. **280**, 39 (2000).

41. M. Balden and J. Roth, *Comparison of the chemical erosion of Si, C and SiC under deuterium ion bombardment*, J. Nucl. Mater. **279**, 351 (2000).

42. U. Fantz and H. Paulin, *Chemical erosion of carbon at low temperatures and low ion energies*, Physica Scripta **T91**, 25 (2001).

43. J. Bohdansky, *A universal relation for the sputtering yield of monoatomic solids at normal ion incidence*, Nucl. Instr. and Meth. B **2**, 587 (1984).

44. C. García-Rosales, W. Eckstein, and J. Roth, *Revised formulae for sputtering data*, J. Nucl. Mater. **218**, 8 (1994).

45. B. V. Mech, A. A. Haasz, and J. W. Davis, *Model for the chemical erosion of graphite due to low-energy H^+ and D^+ impact.*, J. Appl. Phys. **84**, 1655 (1998).

46. P. Sigmund, in *Sputtering by Particle bombardment*, edited by R. Behrisch (Springer, Berlin, 1981), Vol. I, pp. 9–71.

47. M. Nastasi, J. Mayer, and J. K. Hirvonen, in *Ion-solid interactions: fundamentals and applications* (Cambridge University Press, Cambridge, UK, 1995), Chap. 3.

48. J. Roth and W. Möller, *Mechanism of enhanced sputtering of carbon at temperatures above 1200°C*, Nucl. Instr. Meth. Phys. Res. **B7/8**, 788 (1985).

49. B. Söder, J. Roth, and W. Möller, *Anisotropy of ion-beam-induced self-diffusion in pyrolytic graphite*, Phys. Rev. B **37**, 815 (1988).

50. P. Franzen, J. W. Davis, and A. A. Haasz, *Line-of-sight measurements of the radiation-enhanced sublimation of graphite*, J. Appl. Phys. **78**, 817 (1995).

51. E. Hechtl, J. Bohdansky, and J. Roth, *The sputtering yield of typical impurity ions for different fusion reactor materials*, J. Nucl. Mater. **103 & 104**, 333 (1981).

52. C. H. Wu, *Chemical sputtering of graphite and tungsten by oxygen*, J. Nucl. Mater. **145-147**, 448 (1987).

53. D. R. Orlander, W. Siekhaus, R. Jones, and J. A. Schwarz, *Reactions of Modulated Molecular Beams with Pyrolytic Graphite. I. Oxidation of the Basal Plane*, J. Chem. Phys. **57**, 408 (1972).

54. D. R. Orlander, R. H. Jones, J. A. Schwarz, and W. Siekhaus, *Reactions of Modulated Molecular Beams with Pyrolytic Graphite. II. Oxidation of the Prism Plane*, J. Chem. Phys. **57**, 421 (1972).

55. E. Vietzke and A. A. Haasz, in *Physical Processes of the Interaction of Fusion Plasmas with Solids*, edited by W. O. Hofer and J. Roth (Academic Press, San Diego, 1996), Chap. 4.

56. K. Nordlund, E. Salonen, J. Keinonen, and C. H. Wu, *Sputtering of hydrocarbons by ion-induced breaking of chemical bonds*, Nucl. Instr. Meth. Phys. Res. B **180**, 77 (2001).

57. A. Schenk, J. Biener, B. Winter, C. Lutterloh, U. A. Schubert, and J. Küppers, *Mechanism of chemical erosion of sputter-deposited C:H films*, Appl. Phys. Lett. **61**, 2414 (1992).

58. J. Biener, U. A. Schubert, A. Schenk, B. Winter, C. Lutterloh, and J. Küppers, *Modeling the elementary steps of low-pressure diamond deposition*, Advan. Mater. **5**, 639 (1993).

59. J. Biener, U. A. Schubert, A. Schenk, B. Winter, C. Lutterloh, and J. Küppers, *A surface reaction with atoms: hydrogenation of sp- and sp^2-hybridized carbon by thermal H(D) atoms*, J. Chem. Phys. **99**, 3125 (1993).

60. C. Lutterloh, A. Schenk, B. Winter, J. Biener, U. A. Schubert, and J. Küppers, *D(H) atom impact induced Eley-Rideal abstraction reaction toward HD at fully hydrogenated C:H(D) surfaces*, Surf. Sci. **316**, L1039 (1994).

61. A. Horn, A. Schenk, J. Biener, B. Winter, C. Lutterloh, M. Wittman, and J. Küppers, *H atom impact induced chemical erosion reaction at C:H film surfaces*, Chem. Phys. Lett. **231**, 193 (1994).

62. D. M. Goebel, J. Bohdansky, R. W. Conn, Y. Hirooka, K. L. Wai, R. E. Nygren, and G. R. Tynan, *Erosion and redeposition of graphite by hydrogen plasmas*, Fusion Technol. **15**, 102 (1987).

63. E. Vietzke, K. Flaskamp, V. Philipps, G. Esser, P. Wienhold, and J. Winter, *Chemical erosion of amorphous hydrogenated carbon films by atomic and energetic hydrogen*, J. Nucl. Mater. **145-147**, 443 (1987).

64. A. A. Haasz, O. Auciello, P. C. Stangeby, and I. S. Youle, *Ion-induced synergistic effects for CH4 production from carbon under H^+, H^0 and H_2 impact*, J. Nucl. Mater. **128-129**, 593 (1984).

65. E. Vietzke, V. Philipps, and K. Flaskamp, *Chemical reactivity of atomic hydrogen on graphite pre-irradiated by hydrogen and argon ions*, J. Nucl. Mater. **162-164**, 898 (1989).

66. C. García-Rosales and M. Balden, *Chemical Erosion of Doped Graphites for Fusion Devices*, J. Nucl. Mater. **290-293**, 173 (2001).

67. A. Y. K. Chen, A. A. Haasz, and J. W. Davis, *Comparison of the chemical erosion yields of doped graphites*, J. Nucl. Mater. **227**, 66 (1995).

68. M. Balden, *Overview on the effects of dopants on chemical erosion and RES of carbon-based materials*, Physica Scripta **T81**, 64 (1999).

69. C. H. Wu, C. Alessandrini, P. Bonal, H. Grote, R. Moormann, M. Rödig, J. Roth, H. Werle, and G. Vieider, *Overview of EU CFCs development for plasma facing materials*, J. Nucl. Mater. **258-263**, 833 (1998).

70. M. Balden, J. Roth, and C. H. Wu, *Thermal stability and chemical erosion of the silicon doped CFC material NS31*, J. Nucl. Mater. **258-263**, 740 (1998).

71. W. Eckstein, *Computer simulation of ion solid interactions*, Vol. 10 of *Springer Series in Materials Science* (Springer, Berlin/Heidelberg, Germany, 1992).

72. M. P. Allen and D. J. Tildesley, *Computer Simulation of Liquids* (Oxford University Press, Oxford, England, 1989).

73. *Atomic & ion collisions in solids and at surfaces: theory, simulation and applications*, edited by R. Smith (Cambridge University Press, Cambridge, UK, 1997).

74. D. W. Brenner, *Empirical potential for hydrocarbons for use in simulating the chemical vapor deposition of diamond films*, Phys. Rev. B **42**, 9458 (1990).

75. K. Beardmore and R. Smith, *Empirical potentials for C-Si-H systems with application to C_{60} interactions with Si crystal surfaces*, Phil. Mag. A **74**, 1439 (1996).

76. D. Porezag, T. Frauenheim, T. Kohler, G. Seifert, and R. Kaschner, *Construction of tight-binding-like potentials on the basis of density-functional theory: Application to carbon*, Phys. Rev. B **51**, 12947 (1995).

77. M. Elstner, D. Porezag, G. Jungnickel, J. Elsner, M. Haugk, T. Frauenheim, H. Suhai, and G. Seifert, *Self-consistent-charge density-functional tight-binding method for simulations of complex materials properties*, Phys. Rev. B **58**, 7260 (1998).

78. B. J. Alder and T. E. Wainwright, *Phase transition for a Hard Sphere-System*, J. Chem. Phys. **27**, 1208 (1957).

79. K. Nordlund, *Molecular dynamics simulation of ion ranges in the 1 – 100 keV energy range*, Comput. Mater. Sci. **3**, 448 (1995).

80. J. Tersoff, *New empirical approach for the structure and energy of covalent systems*, Phys. Rev. B **37**, 6991 (1988).

81. J. Tersoff, *Empiric interatomic potential for carbon, with applications to amorphous carbon*, Phys. Rev. Lett. **61**, 2879 (1988).

82. J. Tersoff, *Modeling solid-state chemistry: interatomic potentials for multicomponent systems*, Phys. Rev. B **39**, R5566 (1989).

83. M. V. R. Murty and H. A. Atwater, *Empirical interatomic potential for Si-H interactions*, Phys. Rev. B **51**, 4889 (1995).

84. H. U. Jäger and M. Weiler, *Molecular dynamics studies of a-C:H film growth by energetic hydrocarbon molecule impact*, Diamond Rel. Mater. **7**, 858 (1998).

85. W. Zhu, Z. Pan, Y. Ho, and Z. Man, *Impact-induced chemisorption of C_2H_2 on diamond(001) surfaces: a molecular dynamics simulation*, Nucl. Instr. Meth. Phys. Res. B **153**, 213 (1999).

86. R. Smith and K. Beardmore, *Molecular dynamics studies of particle impacts with carbon-based materials*, Thin Solid Films **272**, 255 (1996).

87. A. Krasheninnikov, K. Nordlund, M. Sirviö, E. Salonen, and J. Keinonen, *Formation of ion irradiation-induced atomic-scale defects on walls of carbon nanotubes*, Phys. Rev. B **63**, 245405 (2001).

88. P. Träskelin, E. Salonen, K. Nordlund, A. V. Krasheninnikov, J. Keinonen, and C. H. Wu, *Molecular dynamics simulations of CH_3 sticking on carbon surfaces*, J. Chem. Phys. (2002), submitted for publication.

89. H. U. Jäger and K. Albe, *Molecular-dynamics simulations of steady-state growth of ion-deposited tetrahedral amorphous carbon films*, J. Appl. Phys. **88**, 1129 (2000).

90. K. Nordlund, J. Keinonen, and T. Mattila, *Formation of ion irradiation-induced small-scale defects on graphite surfaces*, Phys. Rev. Lett. **77**, 699 (1996).

91. C. M. Goringer, D. R. Bowler, and E. Hernandez, *Tight-binding modelling of materials*, Rep. Prog. Phys. **60**, 1447 (1997).

92. T. Frauenheim, P. Blaudeck, U. Stephan, and G. Jungnickel, *Atomic structure and physical properties of amorphous carbon and its hydrogenated analogs*, Phys. Rev. B **48**, 4823 (1993).

93. U. Stephan, T. Frauenheim, P. Blaudeck, and G. Jungnickel, *π - bonding versus electronic defect generation: an examination of band gap properties in amorphous carbon*, Phys. Rev. B **50**, 1489 (1994).

94. H. J. C. Berendsen, J. P. M. Postma, W. F. van Gunsteren, A. DiNola, and J. R. Haak, *Molecular dynamics with coupling to external bath*, J. Chem. Phys. **81**, 3684 (1984).

95. J. Roth, B. M. U. Scherzer, R. S. Blewer, D. K. Brice, S. T. Picraux, and W. R. Wampler, *Trapping, detrapping and replacement of keV hydrogen implanted into graphite*, J. Nucl. Mater. **93 & 94**, 601 (1980).

96. B. L. Doyle, W. R. Wampler, and D. K. Brice, *Temperature dependence of H saturation and isotope exchange*, J. Nucl. Mater. **103 & 104**, 513 (1981).

97. G. Federici and C. H. Wu, *Modelling of the interaction of hydrogen plasma with amorphous carbon films redeposited in fusion devices*, J. Nucl. Mater. **207**, 62 (1993), and references therein.

98. E. Salonen, A. V. Krasheninnikov, K. Nordlund, J. Keinonen, and C. H. Wu, *Obtaining distributions of plasma impurities using atomistic simulations*, Contrib. Plasma Phys. **42**, 458 (2002).

99. B. J. Garrison and W. A. Goddard III, *Reaction mechanism for fluorine etching of silicon*, Phys. Rev. B **36**, 9805 (1987).

100. J. Roth, in *Sputtering by particle bombardment*, edited by R. Behrisch (Springer, Berlin, 1981), Vol. II, pp. 91–146.

101. E. Vainonen, J. Likonen, T. Ahlgren, P. Haussalo, and J. Keinonen, *Hydrogen migration in diamond like carbon films*, J. Appl. Phys. **82**, 3791 (1997).

102. S. J. Stuart, A. B. Tutein, and J. A. Harrison, *A reactive potential for hydrocarbons with intermolecular interactions*, J. Chem. Phys. **112**, 6472 (2000).

103. R. Ahlrichs, M. Bär, M. Häser, H. Horn, and C. Kölmel, *Electronic structure calculations on workstation computers the program system TURBOMOLE*, Chem. Phys. Lett. **162**, 165 (1989).